Simulation of Regional Climate Using a Limited Area Model Nested in a General Circulation Model

FILIPPO GIORGI

National Center for Atmospheric Research, Boulder, Colorado*

(Manuscript received 3 November 1989, in final form 26 March 1990)

ABSTRACT

A Limited Area Model (LAM) is nested in a General Circulation Model (GCM) to simulate the January climate over the western United States. In the nesting procedure, the GCM output is used to provide the initial and lateral atmospheric boundary conditions necessary to drive the LAM. In this approach, the GCM is used to simulate realistic large-scale atmospheric behavior over an area of interest and the LAM to describe the effect of local, sub-GCM grid scale forcings (such as those induced by the complex western United States topography) on regional patterns of climatic variables. Two versions of the National Center for Atmospheric Research (NCAR) Community Climate Model [the seasonal CCM1 at 4.5° × 7.5° (R15) and 2.89° × 2.89° (T42) latitude–longitude resolution] are used to drive a version of the Pennsylvania State University/NCAR mesoscale model (MM4 at 60 km resolution), which includes sophisticated soil hydrology calculations. The CCM1 large-scale January climatology over the region is analyzed first. Comparison with large-scale observations shows that geopotential height, zonal wind, temperature, relative humidity, cloudiness, precipitation and storm frequencies over the western United States and adjacent oceans are realistically simulated by both the T42 and R15 models. The T42 model, however, reproduces storm frequencies, and strength and position of the jet stream better than the R15 model. A number of month-long January simulations were performed using both the R15 and T42 model outputs to drive the MM4. The large-scale average circulations over the western United States simulated by the nested MM4 are not substantially different from those of the driving CCM1, both when outputs from the R15 and T42 versions are used to drive the MM4. Owing to the more realistic topography in the MM4, the nested model system produces better regional detail of precipitation and temperature distribution than the CCM1 alone. Temperature and precipitation means, as well as frequencies of daily precipitation intensities simulated by the nested MM4, compare well with high resolution observations, particularly in their spatial distribution. Also discussed are results of regional snow cover, cloudiness, and soil hydrology calculations included in the MM4.

1. Introduction

Recently, Dickinson et al. (1989), Giorgi et al. (1989), and Giorgi and Bates (1989) described the first stages of the development of a nested general circulation model (GCM)–limited area model (LAM) framework for simulation of regional climates. The nested modeling technique consists of using a coarse resolution GCM to carry out simulations of global climate and then employing the GCM output to drive a high resolution LAM over an area of interest. This is a one-way nesting technique in which the circulations produced by the LAM do not feed back into the GCM. The basic idea is that the GCM can provide the correct large-scale circulation response to global climatic forcings, and the LAM can describe the effect of sub-GCM grid scale forcings, due for example to large bodies of water, surface vegetation characteristics, or complex topography and coastlines that may significantly influence the characteristics of local climates.

The main thrust for the development of the nested modeling technique derives from growing interest in predicting regional effects of global climate changes. Indeed, current GCMs are too coarse to resolve local forcings, and due to limitations in both computational resources and representation of relevant physical processes, it may be several years before high resolution GCM simulations become feasible. The nested modeling approach to high resolution regional climate simulation offers two main advantages. The first is the availability of both coarse resolution GCMs that have proven successful in reproducing the basic features of large-scale atmospheric circulations (e.g., Dickinson 1986) and high resolution LAMs that are capable of describing a wide range of mesoscale phenomena (e.g., Anthes 1983). The second is the relative simplicity and effectiveness of the one-way nesting technique (Dickinson et al. 1989). However, the nested modeling methodology is in its infancy, and many of its aspects

* The National Center for Atmospheric Research is sponsored by the National Science Foundation.

Corresponding author address: Filippo Giorgi, National Center for Atmospheric Research, P.O. Box 3000, Boulder, CO 80307.

still need to be thoroughly tested, especially because the use of LAMs for climate studies is entirely new. Examples of relevant issues concerning the feasibility of the nested modeling approach are: (i) Can the nested LAM be run for long simulation times without excessive generation of error?, (ii) Do the synoptic systems simulated by the nested model show realistic features?, and (iii) Does the nested model reproduce accurately the high resolution spatial detail of climate statistics in regions in which sub-GCM grid scale forcings are important?

In a series of recent works, Dickinson et al. (1989), Giorgi et al. (1989), Giorgi and Bates (1989) and Giorgi (1990) began addressing some of these issues by applying a nested GCM–LAM model system over the western United States. The western United States is a region where the nested modeling approach can be especially useful. The local complex topography exerts a strong forcing on, and essentially regulates, the spatial distribution of temperature and precipitation. Because the features of this topography are not captured at the resolution typical of most current GCMs (300–500 km), GCM simulations of climatic variables over the western United States do not yield realistic regional detail. This detail can be achieved with the use of a nested LAM, which can be run at resolutions as low as a few tens of kilometers and can capture the main features of the western United States mountain systems.

The models employed for these studies were versions of the National Center for Atmospheric Research (NCAR) Community Climate Model (CCM) and the Pennsylvania State University/NCAR mesoscale model (version MM4). Both models included a relatively sophisticated surface physics/soil hydrology package (the biosphere–atmosphere transfer scheme, or BATS; Dickinson et al. 1986) for simulating soil hydrologic budgets. Giorgi and Bates (1989) and Giorgi (1990) first tested the performance of the MM4 over the western United States by carrying out a series of month-long wintertime simulations driven by observed fields. Note that this long integration is already an order of magnitude greater than most previous applications of LAMs. They found that the model error did not grow after the first 1–2 days of integration, and that the MM4 captured rather well the local topographic forcing on precipitation. Dickinson et al. (1989) and Giorgi et al. (1989) then simulated six wintertime storms (3–5-day events) with the coupled CCM–MM4 system selected from a three-year CCM simulation. Their results were most encouraging. The simulated storms showed realistic features, and the nesting process did not appear to introduce large errors in the interior of the domain. A January precipitation climatology estimated from the storm sample showed realistic regional detail and was close to high resolution observations over most of the western United States; a surprisingly good result given the small storm sample.

The purpose of this study is to expand on the work of Dickinson et al. (1989) and Giorgi et al. (1989) and to further analyze the performance of the nested CCM–MM4 modeling system for regional climate and hydrology simulation. This paper presents a comprehensive regional climate analysis of the nested model system with a focus, for illustration, on the wintertime (specifically January) climate over the western United States. The analysis consists of the following steps: (i) Given that the prerequisite for a successful regional climate simulation via a nested GCM–LAM model is the capability of the GCM to realistically simulate large-scale circulations over the region, the large-scale climatology over the western United States of different versions of the CCM is first verified against available large-scale observations (section 3); (ii) Month-long simulations with the nested MM4 (i.e., with boundary conditions provided by the CCM output) are performed, and the biases introduced by the nesting procedure are evaluated (section 4). Note that the completion of month-long simulations allows a nested MM4 January climatology to be derived without making use of the simplistic statistical approach of Dickinson et al. (1989); (iii) The nested MM4 and the driving CCM1 regional climatologies are compared in order to estimate the improvements introduced by the nesting approach over the use of the CCM alone (section 4); and (iv) The spatial distribution of various statistics of nested MM4 climatic variables are compared with available high resolution observations to assess how the nested model reproduces the regional climate detail induced by local topographical forcing (section 4). In addition, section 5 discusses the regional hydrologic budgets simulated by the soil hydrology calculations included in the MM4. Individual storms simulated by the nested MM4 are not analyzed in detail here because this was previously accomplished in Dickinson et al. (1989) and Giorgi and Bates (1989).

2. Brief description of models and nesting procedure

The models employed for this study are the standard NCAR CCM (version CCM1) and the augmented version of MM4 described in Giorgi and Bates (1989) and Dickinson et al. (1989). The CCM1 is extensively described in Williamson et al. (1987) and Williamson and Williamson (1987). It is a spectral model capable of seasonally varying simulations. Two versions of the CCM are analyzed, one with a R15 truncation (rhomboidal expansion truncated at wavenumber 15, corresponding to a 4.5° × 7.5° horizontal resolution) and one with a T42 truncation (triangular expansion truncated at wavenumber 42, corresponding to a 2.89° × 2.89° resolution). Both versions include 12 vertical σ-coordinate levels, where $\sigma = p/p_s$, p is pressure, and p_s is surface pressure. Of the 12 vertical levels, five are in the lower stratosphere and seven in the troposphere. Seasonally varying sea surface temperature (SST) and

sea ice distributions are specified from climatological observations, while the snow cover is specified as a function of latitude. Precipitation is obtained from a moist convective adjustment scheme in unstable conditions and from precipitation of supersaturated water in stable environments. Ground temperature is calculated from a surface-energy balance formulation. For both versions, the complex western United States topography is averaged to form a single gently sloping mountain, centered over Utah, of ~1600 m height for the R15 model and ~2000 m height for the T42 model.

The augmented version of MM4 used here couples to the basic dynamical structure described by Anthes and Warner (1978) and Anthes et al. (1987), a Kuo-type cumulus parameterization (Anthes 1977), precipitation of condensed water in stable environments, the detailed radiative transfer scheme of the CCM1 (Kiehl et al. 1987), a medium resolution planetary boundary layer formulation (Giorgi and Bates 1989), and BATS for surface physics–soil hydrology calculations. BATS includes prognostic equations for the temperature of a canopy layer, a surface soil layer of ~10 cm thickness, and root zone layer of 1–2 m thickness. Soil hydrology calculations include explicit prediction of snow depth, soil moisture, and surface runoff and account for the effect of soil freezing. The physics formulations included in BATS are described in detail in Dickinson et al. (1986) and are briefly reviewed in section 5.

The MM4 is a hydrostatic, σ-vertical coordinate model. In the horizontal, a Lambert conformal projection is adopted. The MM4 domain employed in this work is the same as that of Dickinson et al. (1989), which was shown to provide a good balance between model computational cost and representation of regional topographical detail. It covers the western United States and adjacent ocean waters, with a center over the Great Basin, a size of 3000×3000 km^2 and a grid point spacing of 60 km. The MM4 domain and topography are shown in Fig. 1. Although smoother than in reality, the Sierra Nevada and the Rocky Mountains, as well as other smaller systems such as the Cascades and the Wasatch range, are resolved. The SST for the oceanic areas included in the MM4 domain is linearly interpolated from the SST field of the CCM. The MM4 landuse distribution is the same as that of Giorgi and Bates (1989). The model top is at 1 mb, with 16 vertical σ levels, five of which are below $\sigma = 0.8$, six are equally spaced levels between $\sigma = 0.8$ and $\sigma = 0.2$, and five are located above $\sigma = 0.2$ to match the CCM1 vertical level structure there.

The nesting procedure is carried out as follows. To be run, the MM4 requires initial conditions and time-dependent lateral boundary conditions for wind components, temperature, surface pressure and water vapor. For a given simulated time period, these variables are first interpolated onto the MM4 grid from the CCM1 output. The CCM1 output fields are available as snapshots every 12 model hours for the R15 version and every 24 model hours for the T42 version. All quantities are interpolated in the horizontal using a standard bilinear procedure, while in the vertical the interpolation is linear in p for wind and relative humidity, and linear in $\log p$ for temperature. The first set of interpolated fields is used as initial conditions for the MM4 simulation. The MM4 lateral boundary conditions are then supplied following the relaxation technique described in Anthes et al. (1987), which includes a diffusive and a Newtonian term. This requires boundary condition values for wind components, temperature, surface pressure, and water vapor at the four outermost MM4 grid point rows and at each MM4 time step (100 seconds), which are provided via a linear interpolation in time from the CCM1 12- or 24-hourly fields projected on the MM4 grid.

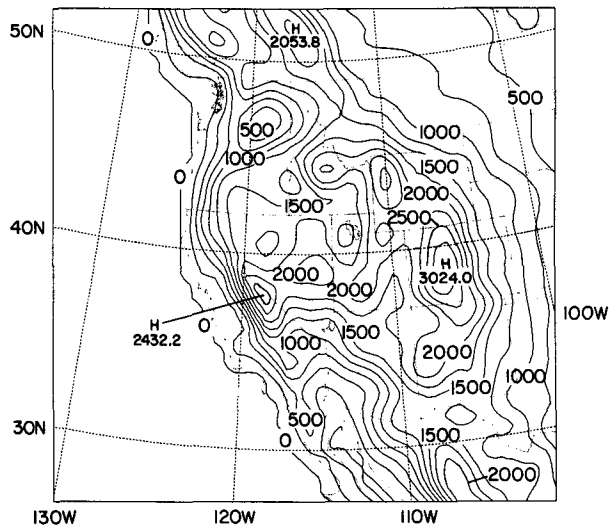

FIG. 1. Topographic field used in the MM4 simulation with a grid point spacing of 60 km. Units are m above sea level and the contour interval is 250 m.

The effect of the frequency of driving-CCM1 field updates was tested in the context of the work of Dickinson et al. (1989), although not discussed in that paper. One of the storms considered by Dickinson et al. (1989) was simulated with the nested MM4 using 6-hourly, 12-hourly, and 24-hourly output from a version of the CCM1 that includes the diurnal cycle. The predicted circulation and precipitation patterns were not sensitive to the frequency of the driving CCM1 output update. Especially for wintertime conditions, this result can probably be expected, since the diurnal cycle is important only near the surface, where the MM4 internal physics mostly dominates (see also section 4). The cases in which the frequency of CCM1 output becomes important occur in the presence of fast disturbances which travel through the nested MM4 domain

in a time period smaller than the CCM1 field update interval. In general, for MM4 domains of a few thousand kilometer size, 12- to 24-hourly CCM1 output should be sufficient to prevent such occurrences.

Another issue of relevance concerns how far into the interior of the domain are boundary conditions dominant over the internal physics of the MM4. This issue was addressed in some detail by Dickinson et al. (1989) and Giorgi and Bates (1989). As already mentioned, the relaxation and diffusive boundary condition terms are gradually applied to the four outermost grid point rows; i.e., using a weighting function that is equal to one at the border of the domain and linearly decreases to zero at the fourth inner grid point (Anthes et al. 1987). The MM4 solution at grid points directly affected by boundary conditions may thus be expected to be dominated by the input from the boundaries.

The effect of the boundary conditions on the interior of the domain depends in general on the speed and direction of the large-scale flow, which determines the advection from the boundaries. Giorgi and Bates (1989) showed that after 24–48 hours of simulation time the effect of the lateral boundary conditions sweeps the whole domain and prevents growth of model error. They also showed that significant mesoscale features associated with local topographic forcings were produced throughout the domain except for the four outermost grid point rows. This internal region of the domain is referred to here as the domain interior, where it can be assumed that the solution reaches a dynamical equilibrium between the information being advected from the boundary and the internal model physics. This equilibrium, in general, will depend on the strength of the advection from the boundaries and the strength of the local forcing.

Concerning the initialization of BATS surface fields, initial canopy and surface soil temperatures are set equal to the initial temperature of the bottom atmospheric model level, the root zone temperature is initialized with the simulation-average of the lowest atmospheric model-level temperature interpolated from the CCM1 output, and the initial snow depth is interpolated from the CCM1 snow depth field, which for January conditions is specified to be equal to one equivalent centimeter of liquid water over land areas north of about 42°N. Finally, initial soil moisture is a function of vegetation type (see Giorgi and Bates 1989 for detail), with soil moisture content close to the wilting point (content at which transpiration ceases) for the semidesert areas of the Southwest, equal to about 30% of saturation for grassy surfaces, and to about 60% of saturation for forested areas. In addition, the soil water content is initialized with its saturation value in areas with initial snow cover different from 0. The saturation water content varies in the range of 0.33 cm/cm of soil for sandy soils to 0.66 cm/cm of soil for clay soils. The soil is assumed to be initially frozen when the initial soil temperature is below 273 K.

3. Analysis of CCM1-simulated January climate over the western United States

January climate over the western United States is dominated by the influence of the Aleutian low and the North Pacific anticyclone. During wintertime, the Aleutian low is strongest and positioned at about 50°–60°N, while the Pacific high is weak and extends from about 30°N over the northeastern Pacific into the continent, where it joins with the thermally induced Great Basin high. As a result, the core of the jet stream is positioned at about 35°–40°N over the northern Pacific. It is then deflected northward along a ridge centered over the continental coasts and reaches its maximum continental value at about 50°–60°N over northeastern Canada. Most of the weather systems affecting the western United States originate over the Pacific, move eastward along the southern edge of the Aleutian low, where they collect oceanic moisture, and impinge upon the coasts of the Gulf of Alaska and the Pacific Northwest. From there, they either dissipate or continue their eastward path over the continent. Less frequently, the jet shifts southward and the Pacific storms enter the California coast and travel across the Southwest.

The first prerequisite for a successful nested GCM–LAM simulation of regional climate is the ability of the GCM to produce a realistic large-scale climatology over the region. Here we compare CCM1-produced January climatological variables at R15 and T42 resolutions with observations at the same or similar scales. Two already available CCM1 simulations were analyzed: a 10-year standard CCM1/R15 seasonal run, and a 6-year standard CCM1/T42 seasonal run. Both runs were initialized with average observed October atmospheric conditions, so that it can be assumed that within a few months the models have reached equilibrium with their specified seasonally varying forcings. In our model verification analysis we consider the mean January 500 mb height, 500 mb temperature, 300 mb zonal wind, and 700 mb relative humidity. The data used for verification of these variables are taken from a European Centre for Medium Range Weather Forecast (ECMWF) global analysis dataset for the years 1979–87 projected on the R15 and T42 CCM1 grids (Trenberth and Olson 1988).

Figures 2–5 show the average January 500 mb height, 500 mb temperature, 300 mb zonal wind, and 700 mb relative humidity over the western United States, western Canada, Alaska, and adjacent oceans (i.e., an area enclosing the MM4 domain and surrounding regions) for the R15 and T42 models and for the ECMWF analysis projected on the T42 grid. The ECMWF analysis fields projected on the R15 grid are not shown because they are almost identical to the corresponding fields on the T42 grid. All model averages shown in this section are taken over all Januaries of the available multiyear seasonal simulations.

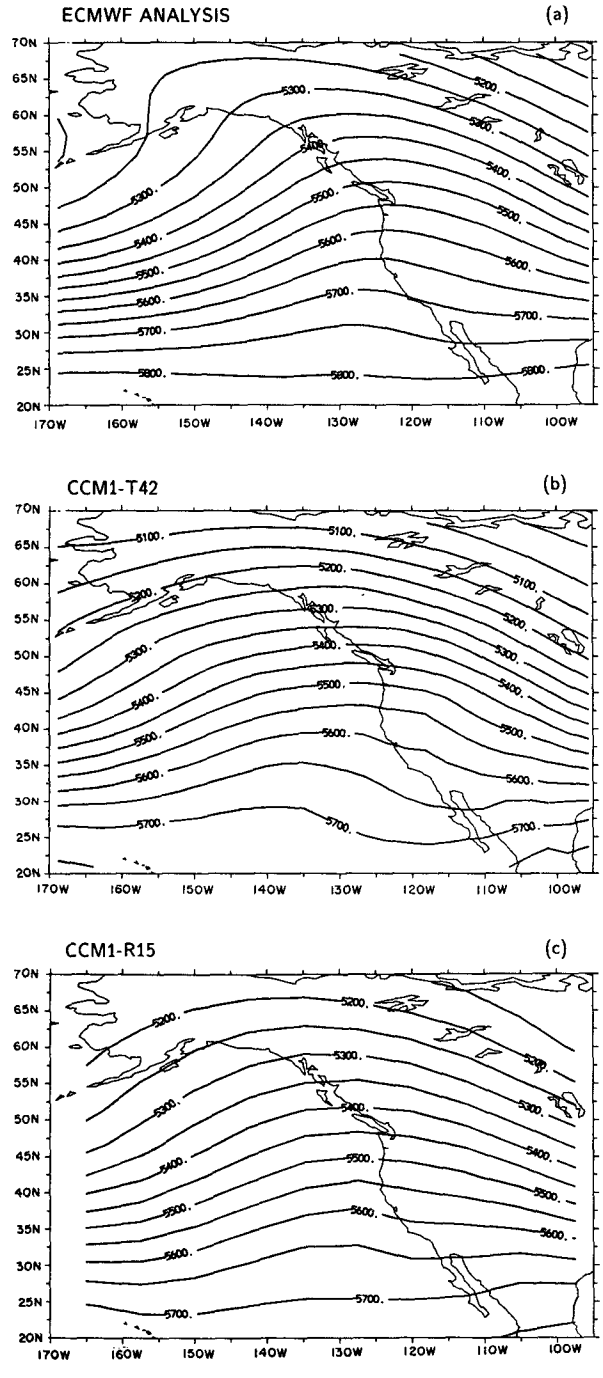

FIG. 2. Average January 500 mb geopotential height: (a) ECMWF analysis projected onto the T42 grid; (b) T42 simulation; (c) R15 simulation. Units are meters and the contour interval is 50 m.

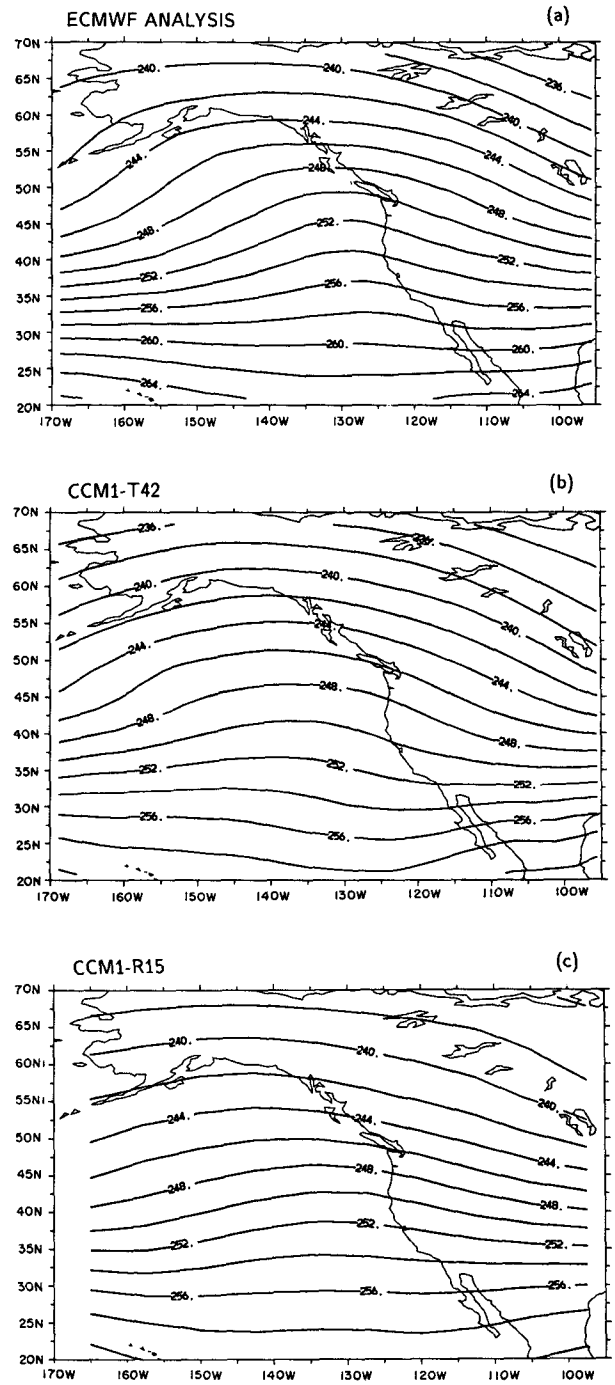

FIG. 3. As in Fig. 2 but for the average January 500 mb temperature: Units are K and the contour interval is 2 K.

Both models capture the 500 mb ridge located at about 120°–130°W, although the ridge is better resolved in amplitude and eastward tilt south of 45°N by the T42 version (Fig. 2). The models underrepresent the sharp westward tilt of the ridge along the Alaskan coast, which results in a northeastern Pacific jet somewhat weaker than in the analysis. This is confirmed by the 300 mb zonal wind (Fig. 4). The simulated core of the jet in the northeast Pacific is weaker than in the analysis by about 10 m s^{-1} for the T42 version and by about 15 m s^{-1} in the R15 version. Also note that in the T42 model the jet impinges upon the continental

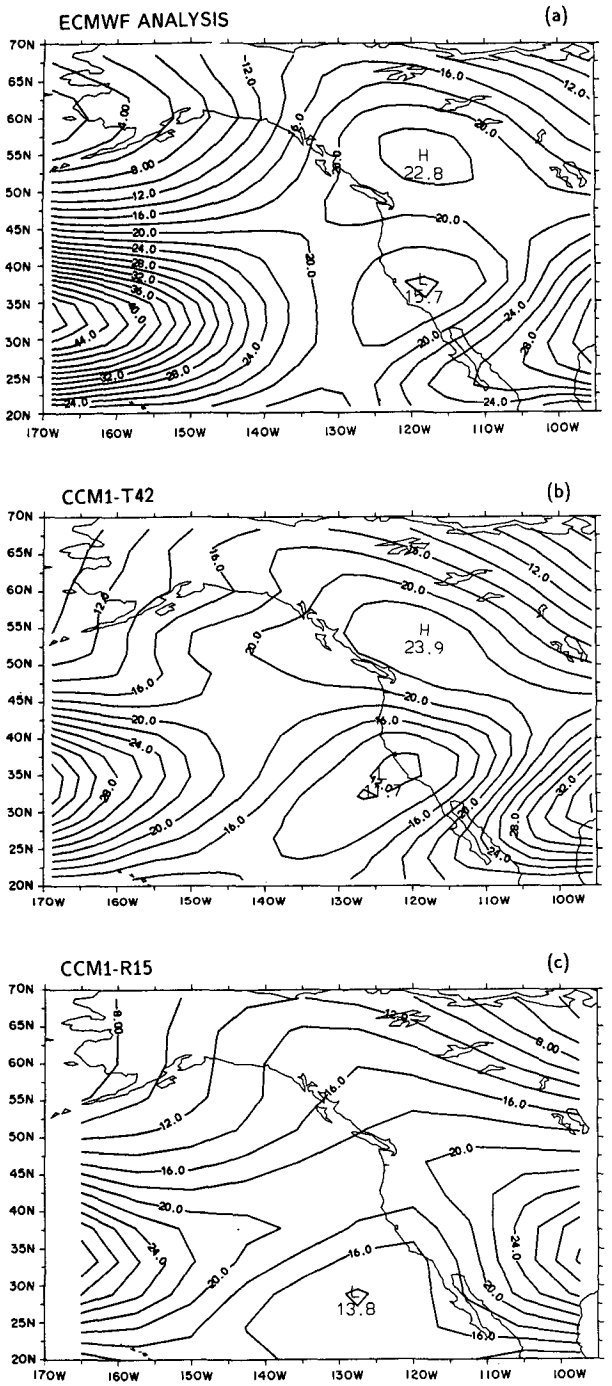

FIG. 4. As in Fig. 2 but for the average January 300 mb zonal wind: Units are m s^{-1} and the contour interval is 2 m s^{-1}.

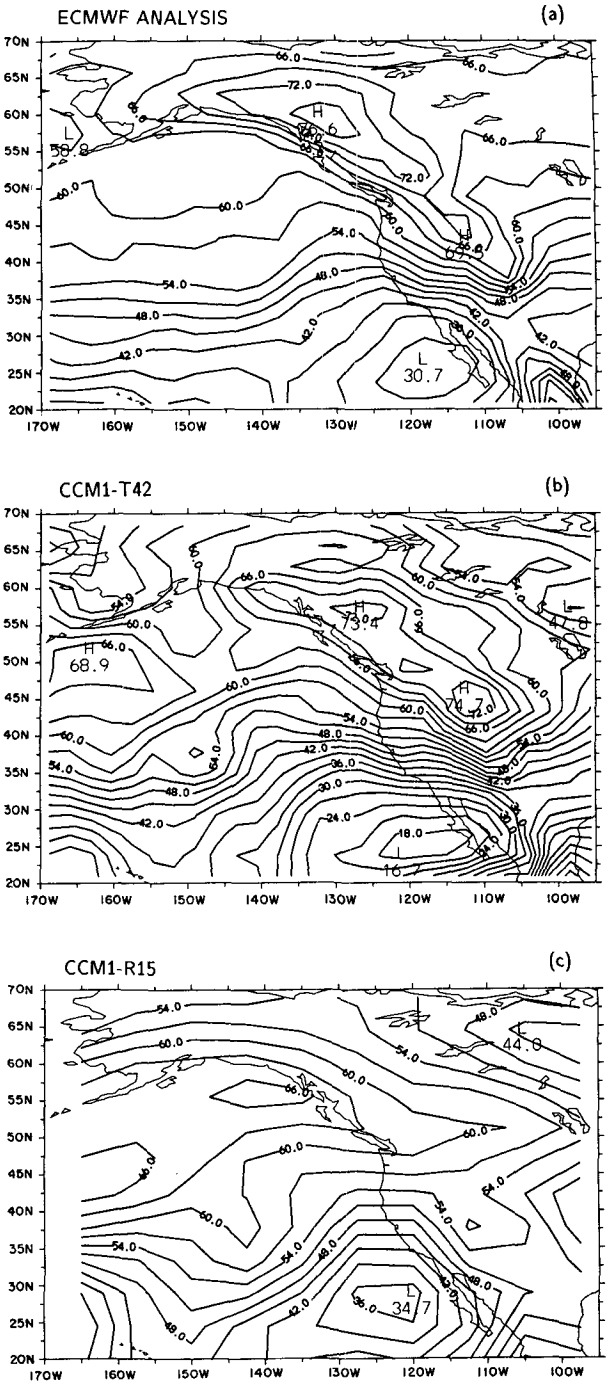

FIG. 5. As in Fig. 2 but for the average January 700 mb relative humidity: Units are percentage of saturation and the contour interval is 3%.

coast at 45°–50°N, which is in agreement with the analysis, while in the R15 model it is displaced southward by about 5°.

The model midtroposphere are colder than in the analysis by 2°–4°C (Fig. 3), a characteristic well known for the standard CCM (e.g., Pitcher et al. 1983). As a consequence, the model 500 mb heights are lower than in the analysis. The southward temperature gradient, and consequently, the baroclinicity of the region, is also somewhat undersimulated by both models. Finally, the T42 version reproduces quite well the main features of the regional low level relative humidity field:

the region of high relative humidity (70%–80%) extending from southern Alaska, along the rockies of Canada, down to the Rockies of Idaho and Wyoming; the sharp southward decrease in relative humidity over the Southwest with a minimum off the coasts of the Baja peninsula; and the general southward decrease over the Pacific. The R15 model also shows these features but positions the region of high relative humidity to the south of that of the analysis (Fig. 5). This result, along with those of Figs. 2 and 4, would suggest that the T42 model predicts well the January storm track over the western United States, while the R15 model positions it somewhat to the south of observations.

To verify this conclusion with independent datasets, model-simulated cyclone tracks and frequencies were estimated. Past studies (e.g., Blackmon et al. 1977; Malone et al. 1984) have inferred storm tracks from the standard deviation of selected time-filtered fields (e.g., 500 mb height). Such analyses, however, do not give information on the frequency of storms but only on the location of areas of high variability within given time and spatial scales. From the viewpoint of climate and hydrology simulation, however, it is important to know if the model can reproduce the correct frequency of storm events.

Available in the literature are a number of compilations of cyclone tracks and frequencies over the continental United States and adjacent oceans (Hosler and Gamage 1956; Klein 1957; Reitan 1974, 1980; Zishka and Smith 1980). The basic technique used to generate these compilations consists of dividing an area of interest into a number of regularly spaced grid boxes and counting, from standard surface weather maps, the number of cyclone centers passing through a given box. A similar procedure was adopted here for the model output.

The CCM1 domain between 20° and 70°N, 100° and 170°W; i.e., the same area as that of Figs. 2–5, was divided into 5° × 5° latitude–longitude boxes, a box size comparable with the model resolution. Maps of sea level pressure were produced over this domain for each model output (i.e., every 12 hours for the R15 version and every 24 hours for the T42 version) with a contour interval of 4 mb. The location of a cyclonic system was identified by the center of the innermost closed isoline around a low pressure center. The trajectory of a system was then obtained by connecting with a straight line the locations of low pressure centers at successive outputs, and the number of storm trajectories crossing each 5° × 5° box was counted. No trajectory was counted more than once for each box, regardless of how long a low pressure center persisted in, or crossed, a given box. No adjustment was made for different areas of boxes at different latitudes (Taylor 1986). Note that this procedure, although somewhat subjective in nature, is the same as that adopted by Hosler and Gamage (1956), Reitan (1974), and Zishka and Smith (1980), and thus allows a meaningful comparison with these works. Also, some error can result from the pressure extrapolation to sea level in mountainous areas.

Figure 6 shows the average January cyclone frequencies (number of cyclone centers per January passing through a given box) calculated for the T42 and R15 models on the grid described above. Also indicated are major (solid arrows) and minor (dashed arrows) storm tracks. These were subjectively estimated by superposition of individual cyclone trajectories. In the T42 model the main storm track enters the domain from the Pacific at about 45°–55°N and impinges upon the western coasts on the Gulf of Alaska. Some storms dissipate there, but a large number continue their eastward motion with a trajectory arching around the northern Rockies and ending over the Great Plains. Although more difficult to detect, some cyclogenesis was noted in the lee of the northern and central Rockies. A minor track originates over the northeastern Pacific, enters the northern California and Pacific North-

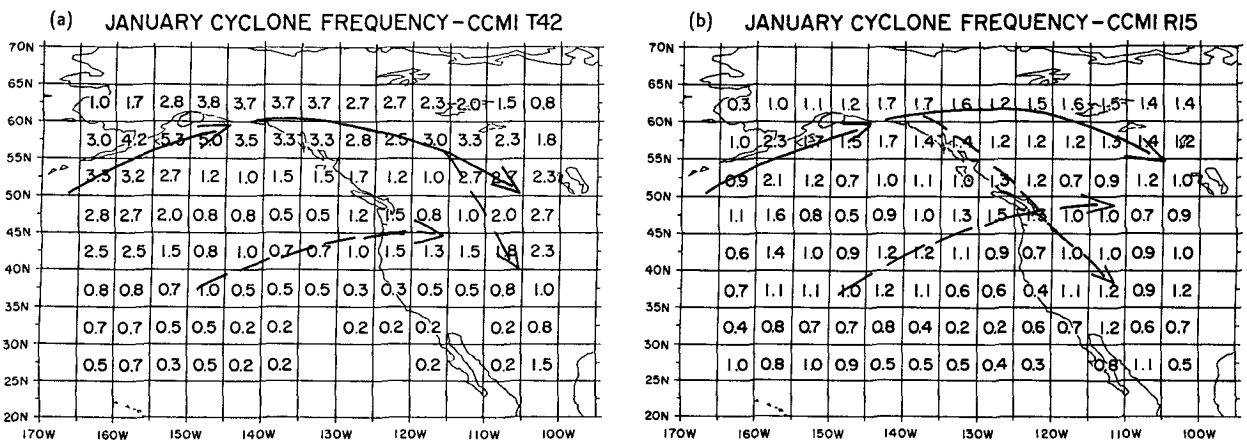

FIG. 6. Average January cyclone frequencies calculated for (a) the T42 model and (b) the R15 model. Units are number of cyclone centers crossing a 5° × 5° grid box per January. Also shown are major (solid arrow) and minor (dashed arrow) cyclone tracks.

west coasts, and crosses the Southwest. The storm tracks are consistent with the tracks provided by Klein (1957) and Zishka and Smith (1980).

The R15 simulation shows the same storm track features as the T42 one, but the Alaskan track is much less pronounced, as indicated by the lower cyclone frequencies, and the California–Pacific Northwest track is more pronounced. This is consistent with the southward shift of the jet indicated by Figs. 2–5. Also note that in general the R15 model produces a smaller number of cyclones than the T42 model.

The cyclone frequencies of Fig. 6 can be compared with the compilation of Zishka and Smith (1980) reported in Fig. 7, which shows the total number of observed cyclone centers (defined with the same procedure as in this work) crossing 2° × 2° grid boxes during 28 Januaries from 1950 to 1977. Assuming that the cyclone centers maintain an eastward motion, the ratio of the number of cyclone centers crossing a 5° × 5° box and the number of those crossing a 2° × 2° box is about 2.5, which is the ratio of the east–west cross-sectional areas of the boxes. Therefore, the frequencies of Fig. 7 can be compared with those of Fig. 6 if we divide them by a factor of 28/2.5 ~ 10. Within the limitations of this procedure, the agreement between the observations of Fig. 7 and the T42 model results is quite good. The Gulf of Alaska maximum of 4–5 cyclones per January is captured, as well as the secondary maximum over the northern plains and the general southward decrease in storm frequencies. The model seems to produce too few cyclones over the southern plains, which is an area of significant cyclogenesis. This is probably due to the model underrepresentation of the Rockies. A similar conclusion; i.e., good agreement over the western and northern United States but underprediction of cyclones in the southern and central plains, is drawn from the comparison (not shown) with the compilations of Hosler and Gamage (1956) and Reitan (1974).

Comparison of Figs. 6b and 7 shows that the R15 simulation tends generally to underpredict the number of cyclones. This may be due to the definition of cyclone center adopted here in relation to the coarse resolution of the R15 model. More important is the southward shift of the storm paths shown in the R15 simulation, which leads to an underprediction of Alaskan storms and overprediction of southwestern storms.

The trends indicated by the storm frequency analysis are reflected in the mean January precipitation. Figure 8 compares the R15 and T42 mean January precipitation with the large-scale observational dataset of Shea (1986). This dataset contains January precipitation averaged over 2.5° × 2.5° grid boxes; i.e., at a resolution close to that of the T42 model. The T42 simulation captures quite well, both in location and intensity, the band of precipitation maxima extending from the Gulf of Alaska to the Pacific Northwest and the sharp westward and southwestward precipitation gradients, with precipitation below 5 cm in the Southwest and below 2.5 cm over the Great Plains. The R15 shows a similar pattern, but the region of coastal precipitation maxima extends farther south than observed, and precipitation over the Southwest and the Great Plains is too large.

Related to precipitation is cloud cover. Figures 9a–c

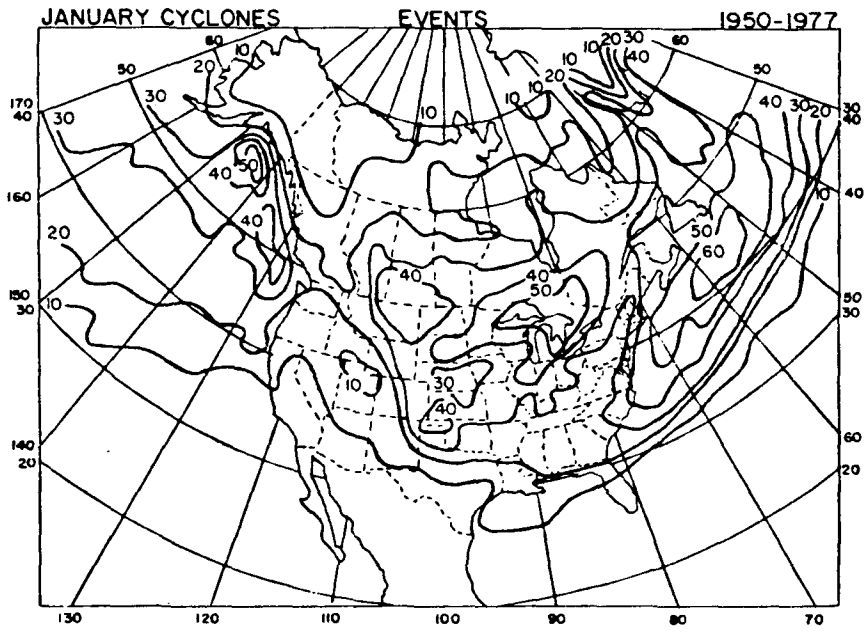

FIG. 7. Observed total number of January cyclone centers crossing 2° × 2° grid boxes in 28 years of observations (1950–77, from Zishka and Smith 1980).

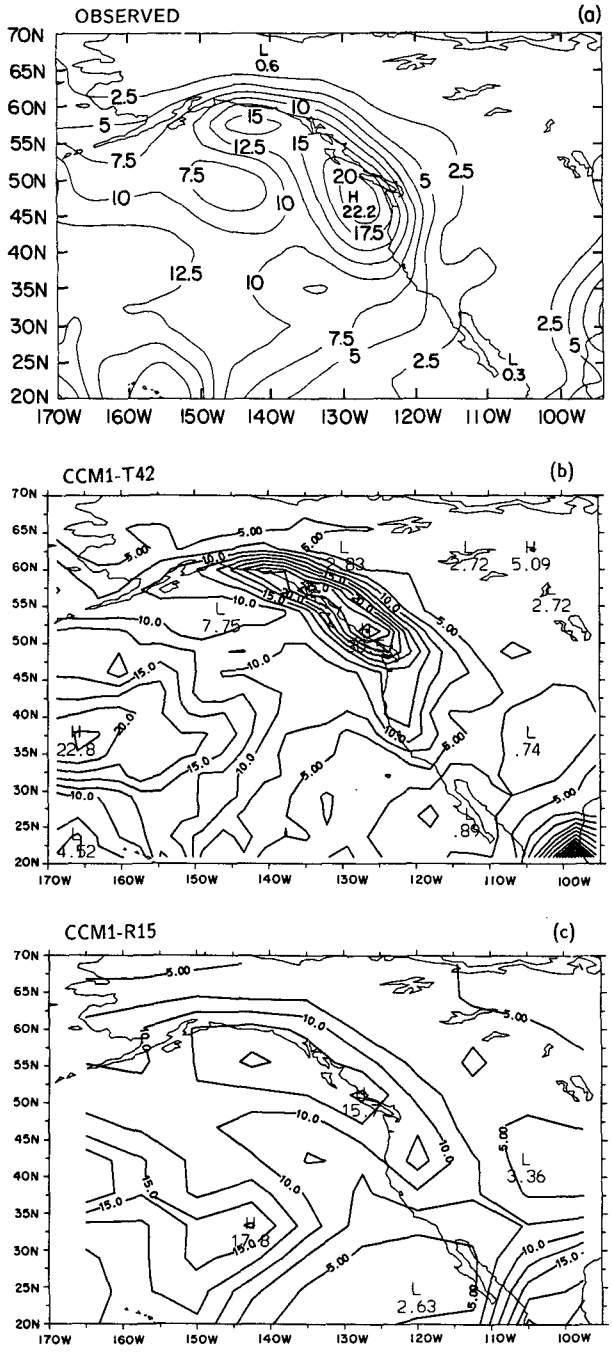

FIG. 8. Average total January precipitation: (a) Observations, (b) T42 model; (c) R15 model. Units are cm and the contour interval is 2.5 cm.

compare the January average total fractional cloud cover for the T42 and R15 simulations with the observational dataset of Warren et al. (1986). This dataset is based on ten years (1971–81) of ground-based observations over land, and the fractional cloud cover is reported in percentage on a 5° × 5° latitude–longitude grid. Note that the CCM1 clouds are calculated by assuming 95% cloud cover in saturated grid points and a total column cover of 30% for layers in which convective precipitation occurs (see section 2). The total fractional cloud covers of Figs. 9b,c are calculated using the random overlap assumption, which is also employed in the radiative transfer calculations (Ramanthan et al. 1983).

Both models show a maximum in the average fractional cloud cover over the Gulf of Alaska and the Pacific Northwest coasts, although this is somewhat underpredicted compared to observations. In the T42 run the cloud cover decreases sharply eastward and southward and is underpredicted over the eastern Great Plains, southern California and Arizona, and northern Mexico by up to 30%–40%. Conversely, in accord with observations, the R15-produced cloud covers are in the range of 30%–50% there. Comparison of cloud and precipitation amounts would suggest that in areas where the models correctly predict precipitation, cloud amounts are somewhat underpredicted. Contributing to this is the absence in the model of fair weather cloudiness formulations (e.g., Ramanathan et al. 1983).

Finally, Fig. 10 compares the average January model air temperature at the lowest sigma level (~70 m height) with the 2.5° × 2.5° resolution observed climatic surface air temperatures of Shea (1986). Because their surface physics formulations and SST fields are the same, the two model versions show similar temperature fields. The main difference occurs over the Great Plains, where the T42 version is colder than the R15 by a few degrees, and over the Rockies, which are better resolved in the T42 model. For both models the temperatures compare reasonably well with observations, particularly in coastal areas that are more directly affected by the specification of the SST. The continental interiors are colder than observed by a few degrees.

Summarizing, both models capture the basic large-scale January climate over the western United States. The T42 version simulates better than the R15 the strength and position of the jet, storm tracks and frequencies, and large-scale precipitation distribution. These results indicate that the CCM output provides a realistic large-scale climatology for MM4 nesting. In Dickinson et al. (1989) and Giorgi and Bates (1989) it was shown that, given good large-scale initial and lateral boundary conditions, the MM4 is able to simulate realistic storm systems and to capture the main effects of local topography. This indicates that the nested model should be able to simulate realistic regional climatic patterns. Discussion and verification of the high resolution January climatology of the nested CCM–MM4 model is presented in the next section.

4. Analysis of nested MM4-simulated January climate over the western United States

To infer nested MM4 January climate statistics over the western United States, the six Januaries of the T42

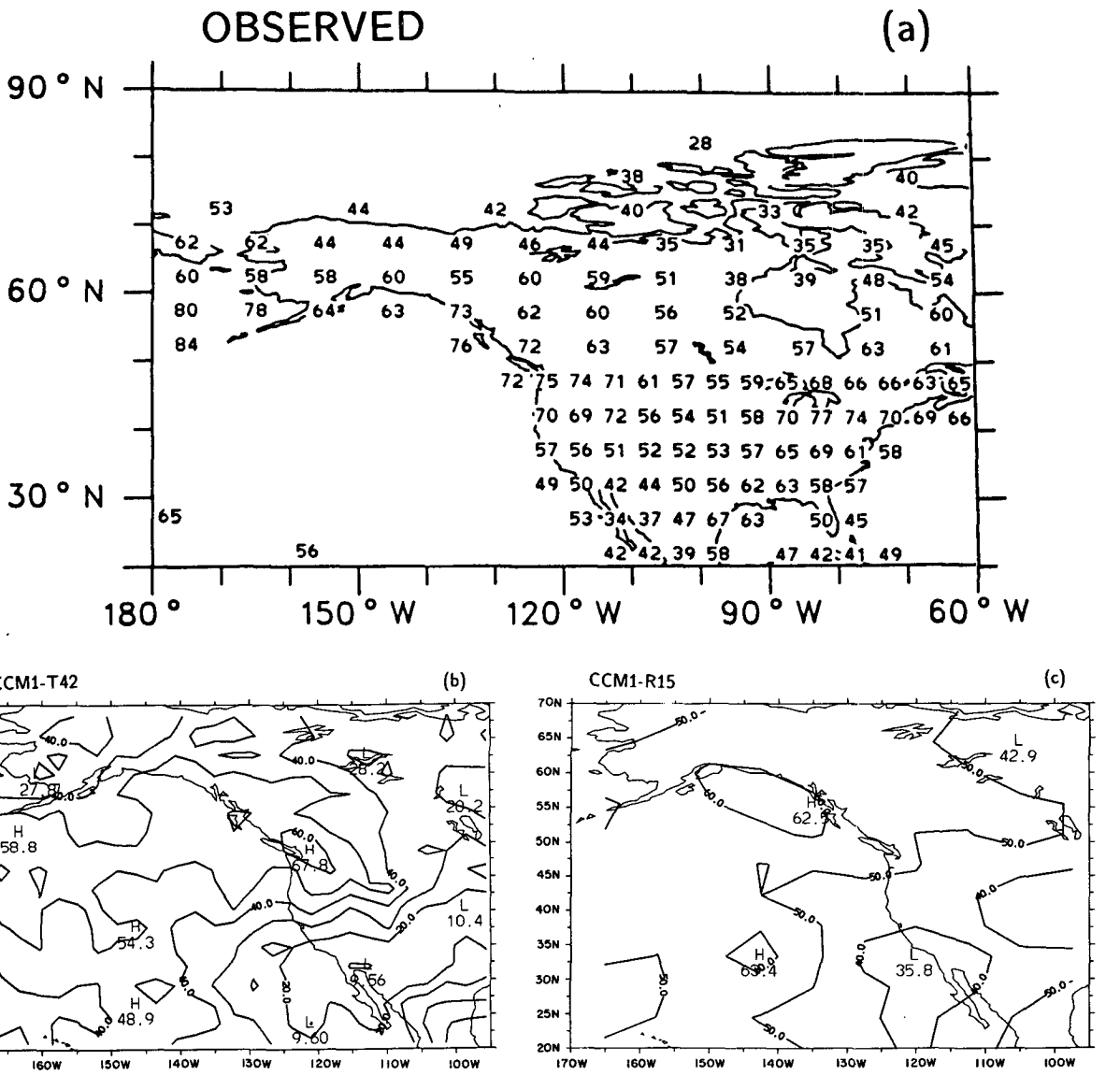

FIG. 9. As in Fig. 8 but for the average January fractional cloud cover: Units are % and the contour interval in the model cloud covers is 10%.

run and the first six Januaries of the R15 run were simulated using the nested model described in section 2, i.e., with initial and lateral boundary conditions provided by the T42 and R15 model, respectively. The nested MM4 January simulations begin at 0000 UTC 1 January and end at 0000 UTC 31 January, of each January.

The first problem to be addressed is whether the nested MM4 large-scale climate over the region substantially deviates from that of the driving CCM1. A measure of this deviation is the bias between nested MM4-produced and -driving CCM1 variables. Here the bias for a given variable (e.g., temperature, wind, and water vapor) at a given vertical level is defined as the difference between the time and horizontal average of the variable as predicted by the MM4 and the same average as obtained by interpolation of the driving CCM1 fields onto the MM4 grid. The horizontal average is taken over the interior of the MM4 domain, i.e., excluding the outermost four grid points which are directly affected by the lateral boundary condition term (see section 2). The time averages are taken over all the Januaries simulated with the nested model using daily (for the T42) or 12-hourly (for the R15) output for the CCM1 interpolated fields and 6-hourly output data for the MM4-produced fields. The latter procedure averages over the diurnal cycle included in the MM4.

Figures 11a–c show the vertical bias profiles as a function of σ for temperature, zonal wind, and water vapor over land and ocean areas. Ocean surface covers

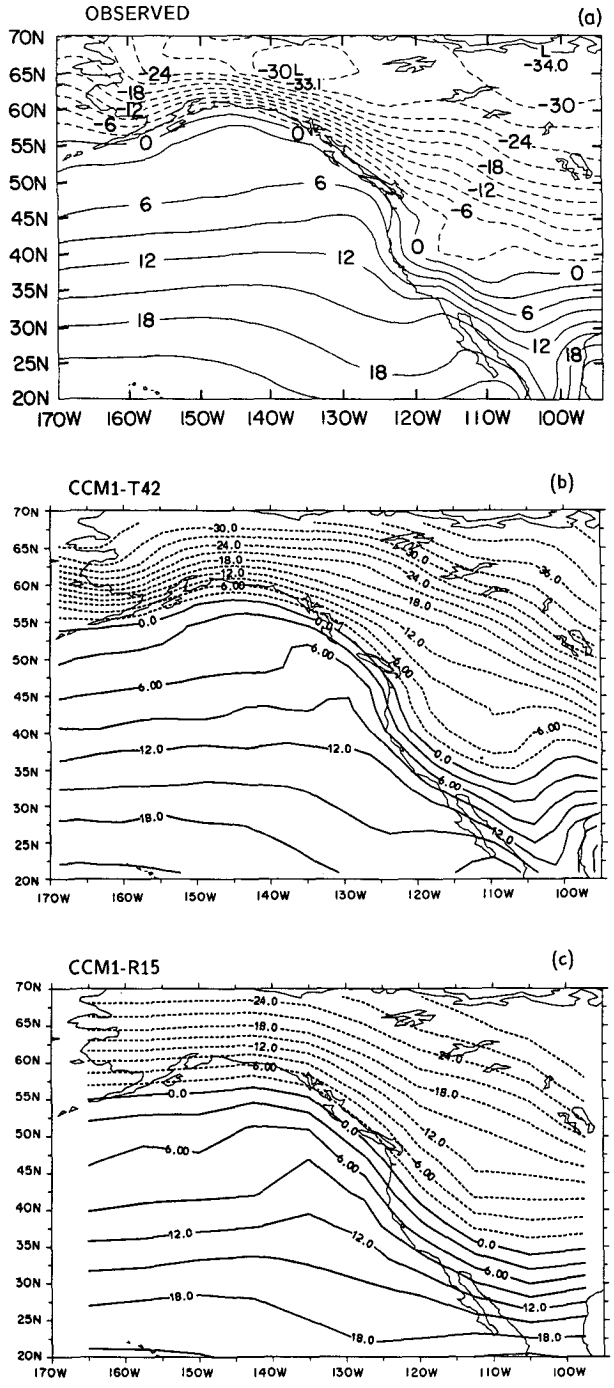

FIG. 10. As in Fig. 8 but for the average January surface air temperature: Units are °C and the contour interval is 3°C.

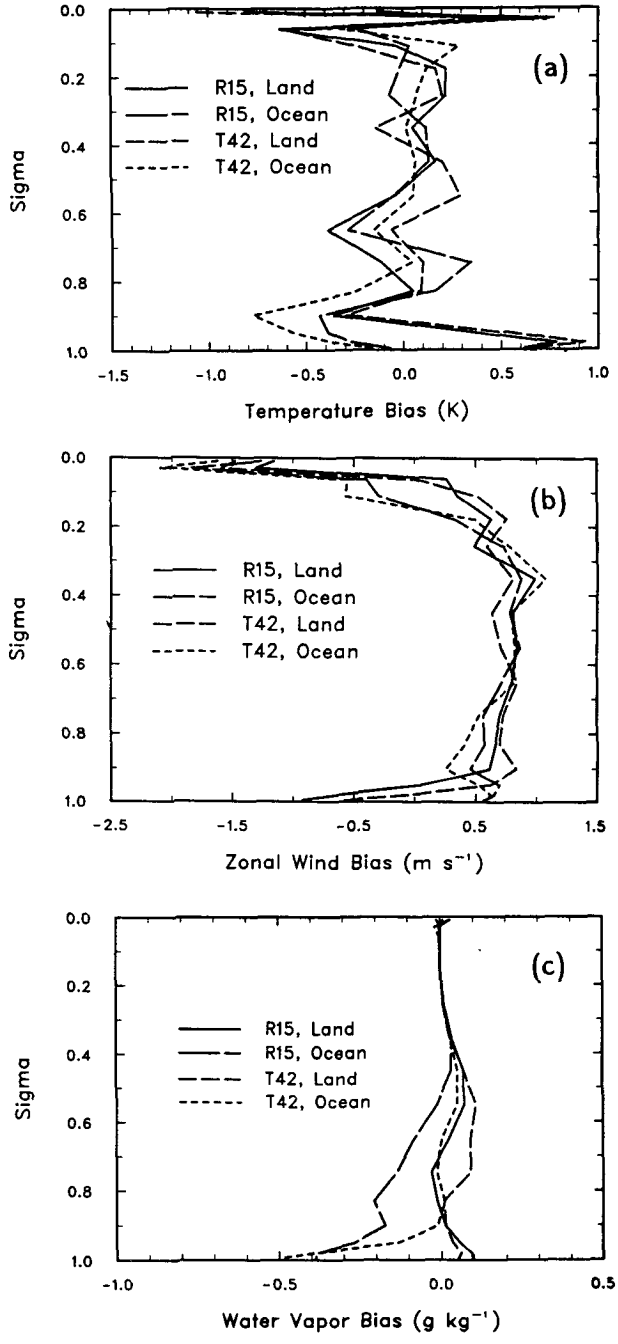

FIG. 11. Average January nested MM4 bias (see text) as a function of σ for the T42-driven and the R15-driven simulations over land and ocean areas for (a) temperature, (b) zonal wind, and (c) water vapor.

about one-third of the whole MM4 domain and land surface the remaining two-thirds. Note that in Giorgi and Bates (1989) it was shown that the basic structure of the bias profiles is reached after 1–2 days of model time, that this structure is kept throughout the simulation with a relatively low degree of variability, and that the biases do not tend to increase with time. This implies that the model solution in the interior of the domain quickly reaches a dynamical equilibrium between the information entering the domain from its lateral boundaries and that deriving from the internal model physics.

Two features can be immediately recognized. First, the biases for the R15 and T42 runs are generally close to each other. This implies that the nesting procedure is not sensitive to the scale of the driving GCM, at least within the range considered here, in terms of mean (climatic) error generation. Second, the biases are larger near the top and bottom model boundaries than in the middle troposphere. This can be expected in view of the fact that local topographical effects near the ground and the presence of the impermeable upper boundary near the model top probably dominate the MM4 solution. Conversely, in the middle troposphere, where synoptic scale dynamics becomes more relevant, advection from the lateral boundaries is increasingly important.

The temperature bias in the midtroposphere is small, less than a few tenths of a degree, while in the boundary layer the nested MM4 is warmer than the CCM1 over land and colder over ocean. This indicates weaker MM4 vertical heat transport in the marine boundary layer. Given that the MM4 and CCM1 boundary layer formulations are similar, this is probably due to the finer MM4 vertical resolution (the MM4 has five levels below $\sigma = 0.8$ while the CCM1 has three levels). Over land the different topographies and surface physics formulations for the two models also contribute to the bias.

The zonal wind bias is consistently positive throughout the troposphere (Fig. 11b). This was confirmed by analyzing the development of individual storm episodes, which showed that many perturbations traveled eastward across the MM4 domain faster in the nested MM4 simulations than in the corresponding CCM1 output. This is likely to be an effect associated with the different model grid scales. The finer MM4 resolution allows the propagation of smaller and faster modes which are filtered out at the coarser CCM1 resolutions. Analysis of the 300 mb zonal wind shows that the jet is stronger in the MM4 than in the CCM1, especially over the southwestern states and adjacent waters, where the average MM4 January zonal wind speed exceeds that of the CCM1 by 1–2 m s^{-1}. A consequence of the faster westward motion of the synoptic systems in the nested MM4 compared with those of the driving CCM1 is that in some instances they appear to "collide" against the eastern (downwind) lateral boundary of the MM4 domain, thereby inducing localized precipitation in the vicinity of the boundary.

Concerning the water vapor bias, both for the T42 and R15 simulations, the nested MM4 is drier than the driving CCM1 over ocean (Fig. 11c). Consistent with the slower MM4 boundary layer vertical transport inferred from the temperature bias profile of Fig. 11a, this is likely due to smaller evaporation rates and weaker vertical moisture transfer in the MM4. Over land the biases are small, less than 0.1 g kg^{-1} throughout the troposphere.

Finally, Figs. 12a,b show the difference in average January 500 mb geopotential height between the nested MM4 and the driving CCM1 interpolated onto the MM4 grid for the six T42 and R15 simulated Januaries. (Note that Figs. 12a,b, as well as all figures which present MM4 results, do not include the outermost grid point shell, where the solution is entirely given by the lateral boundary conditions). It is evident that for both cases the large-scale patterns of the average 500 mb height are essentially unaltered by the MM4 nesting, with height differences reaching ~25 m only over the tallest MM4 topographical features. This result, along with the small midtropospheric biases of Fig. 11,

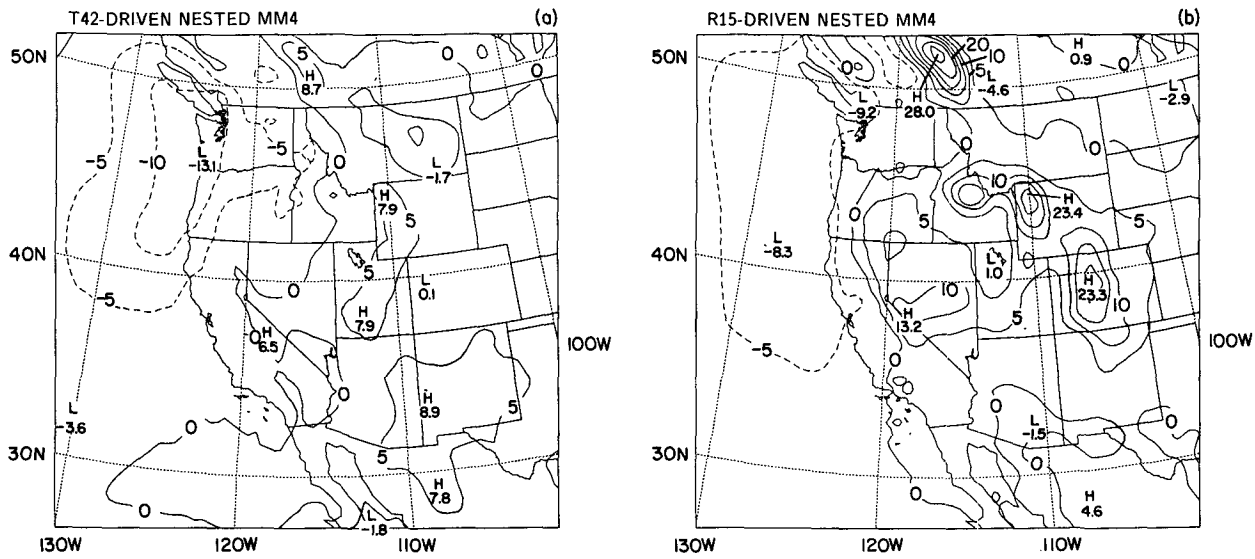

FIG. 12. Difference in average January 500 mb geopotential height between nested MM4 simulation and driving CCM output interpolated onto the MM4 grid: (a) T42-driven simulation, (b) R15-driven simulation. Units are m and the contour interval is 10 m.

illustrate how the basic features of the climatology of the large-scale flow over the region, as simulated by the nested MM4, are essentially the same as those of the driving CCM1. This would suggest that if the GCM-produced large-scale driving climatology over a region is unrealistic, the nested LAM climatology, likewise, would be unrealistic. Further work, however, comparing the use of different quality GCM input for the same cases, is needed to test the generality of this conclusion.

While the MM4 nesting does not substantially alter the large-scale climatology over the region, it strongly modifies the prediction of the regional distribution of quantities such as temperature and precipitation, which depend on topographical features that are captured at the MM4 resolution but are lost at the CCM resolution (see section 2). In the remainder of this section we analyze the influence of local topographical effects simulated by the nested MM4 on sub-CCM grid scale regional patterns of climatic variables.

We first examine surface air temperature. Figure 13 compares observed average January surface air temperature with the average temperature predicted at the bottom atmospheric level of the nested MM4 ($\sim$40 m height) for the R15- and T42-driven simulations. The observed data are taken from a high resolution ($0.5° \times 0.5°$) dataset recently generated by Legates and Willmott (1990a). The data are shown on their original grid, i.e. a regular latitude–longitude grid, instead of the MM4 grid to avoid interpolation and averaging procedures that would alter them. The January model temperatures are obtained by averaging over six-hourly MM4 model output and over all simulated Januaries.

The agreement between models and observations is good over coastal areas, and the 0°C model isotherm is well positioned. In the continental interiors, both nested model simulations capture high resolution topographically induced temperature patterns not present in the coarse scale CCM results (see Fig. 10). For example, the orographic cooling over the Sierra Nevada and Rocky mountains is well simulated, especially in the R15-driven simulation, while the T42-driven simulation is a few degrees colder than observations and R15-driven results over the Great Basin and other areas of the Southwest. This can probably be attributed to the location of the average model storm path, which in the R15 run, is shifted southward with respect to the T42 run and thus induces advection of warmer oceanic air over continental regions.

More so than temperature, precipitation over the western United States is strongly affected by the local topography. Figure 14a reports mean observed January precipitation taken from the $0.5° \times 0.5°$ resolution dataset of Legates and Willmott (1990b). The effect of topography on precipitation is quite evident. Strong precipitation maxima, in excess of 20 cm, are observed over the coastal ranges, the Sierra Nevada, and the Cascade Range, with secondary maxima over the northern Rockies of Idaho (over 10 cm), the central

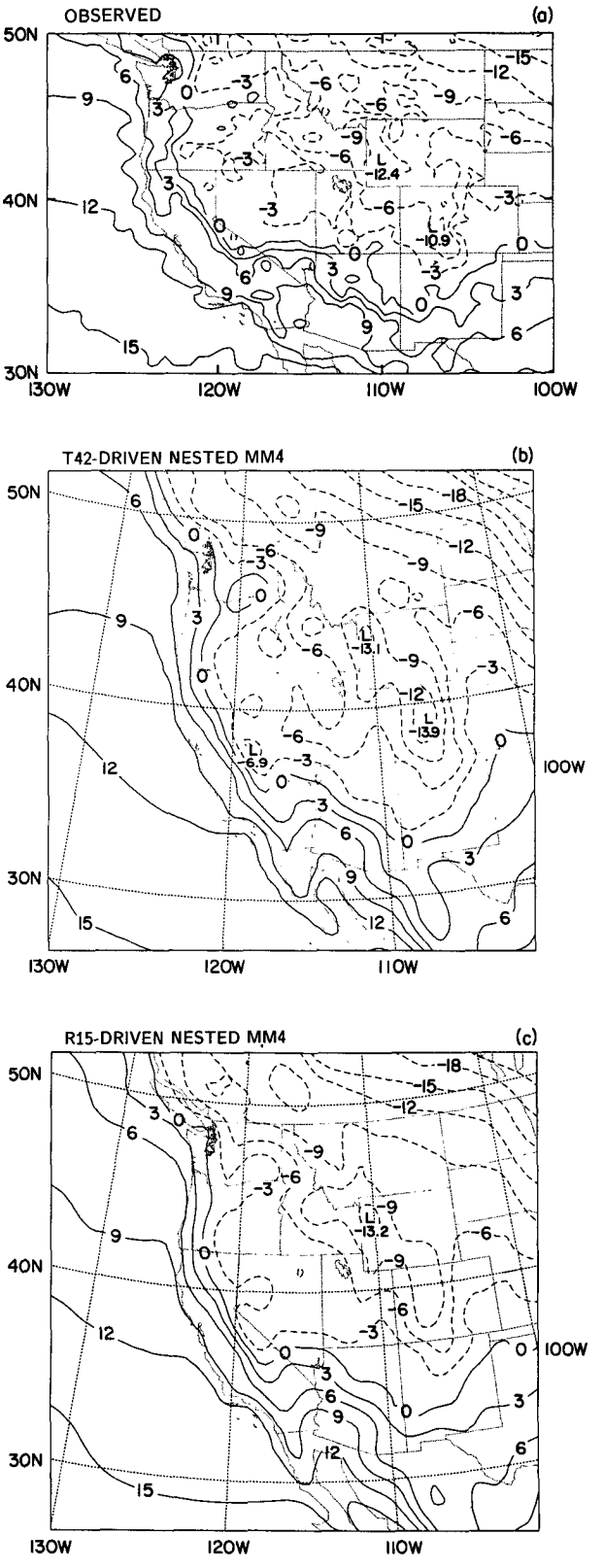

FIG. 13. Average January surface air temperature: (a) Observations, (b) T42-driven nested MM4, and (c) R15-driven nested MM4. Units are °C and the contour interval is 3°C.

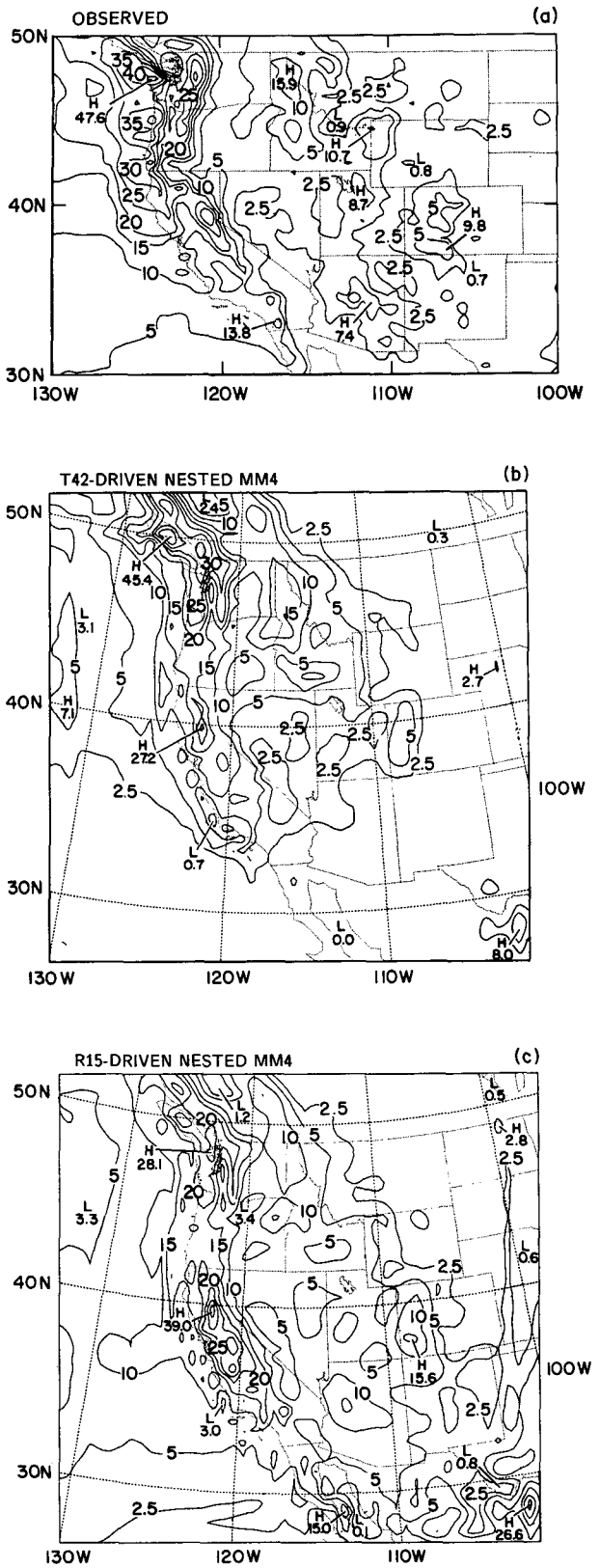

FIG. 14. As in Fig. 13 but for the average total January precipitation: Units are cm and the contour interval is 5 cm.

Rockies of Colorado (over 5 cm), and the southern Rockies of Arizona (over 5 cm). Other secondary maxima are found over the Wasatch Range in Utah and the southern California mountains. The maxima are generated by orographic upslope motion within the eastward moving Pacific storm systems. Dry conditions are induced over the Great Basin by the precipitation shadowing effect of the Sierra Nevada and the coastal ranges. It is evident from the comparison of Figs. 8b,c and Fig. 14a that neither GCM captures this regional detail in the precipitation field.

Figures 14b,c show the average January precipitation for the nested MM4 simulations. Note that the average precipitation amounts for the first six years of the 10-year R15 run (not shown) follow the same spatial pattern, but are larger (by ~20%) than those of the remaining four. Therefore, the precipitation means shown in Fig. 14c are probably larger than they would be if all ten Januaries of the R15 run had been simulated with the nested MM4. Comparison of Figs. 14a,b,c shows that the nested MM4 captures most regional features of observed average precipitation. For the T42 run (Fig. 14a), primary maxima over the Sierra Nevada, coastal ranges, and Cascades, as well as secondary maxima over the northern and central Rockies and Wasatch Range are well reproduced, both in location and amount. The dry conditions over the Great Basin, with extended areas of precipitation below 2.5 cm, are also well simulated. However, the model is too dry over Arizona and southern California, most likely because of underprediction of southern storms (see also section 3).

Because, as already discussed, the R15 run yields a southward displacement of the jet, which induces too many storms over the Southwest, the R15-driven nested MM4 model tends to overpredict precipitation there. However, the location of the simulated maxima associated with the western Colorado Rockies, central Arizona Rockies, and southern California ranges is in agreement with observations, which illustrates the ability of the MM4 to describe local effects of these mountainous systems. Overall, Figs. 14b,c show that the MM4 effectively simulates the high resolution spatial structure of the average January precipitation field as affected by local topographical effects.

In addition to climatic means, climatic variability is of considerable interest for the evaluation of climatic impact on ecosystems and hydrology (e.g., Mearns et al. 1984, 1990). Therefore, it is important to verify the model's ability to simulate not only climatic averages but also higher statistical moments of climatic variables, e.g., frequency of occurrence of given events. As an example of such a verification analysis, Figs. 15–17 compare the average model-predicted number of days per January with precipitation in excess of 0.25, 1.25, and 2.5 cm, respectively, with observed station data. The data are taken from Climates of the States (1985a,b), where the number of days is reported with

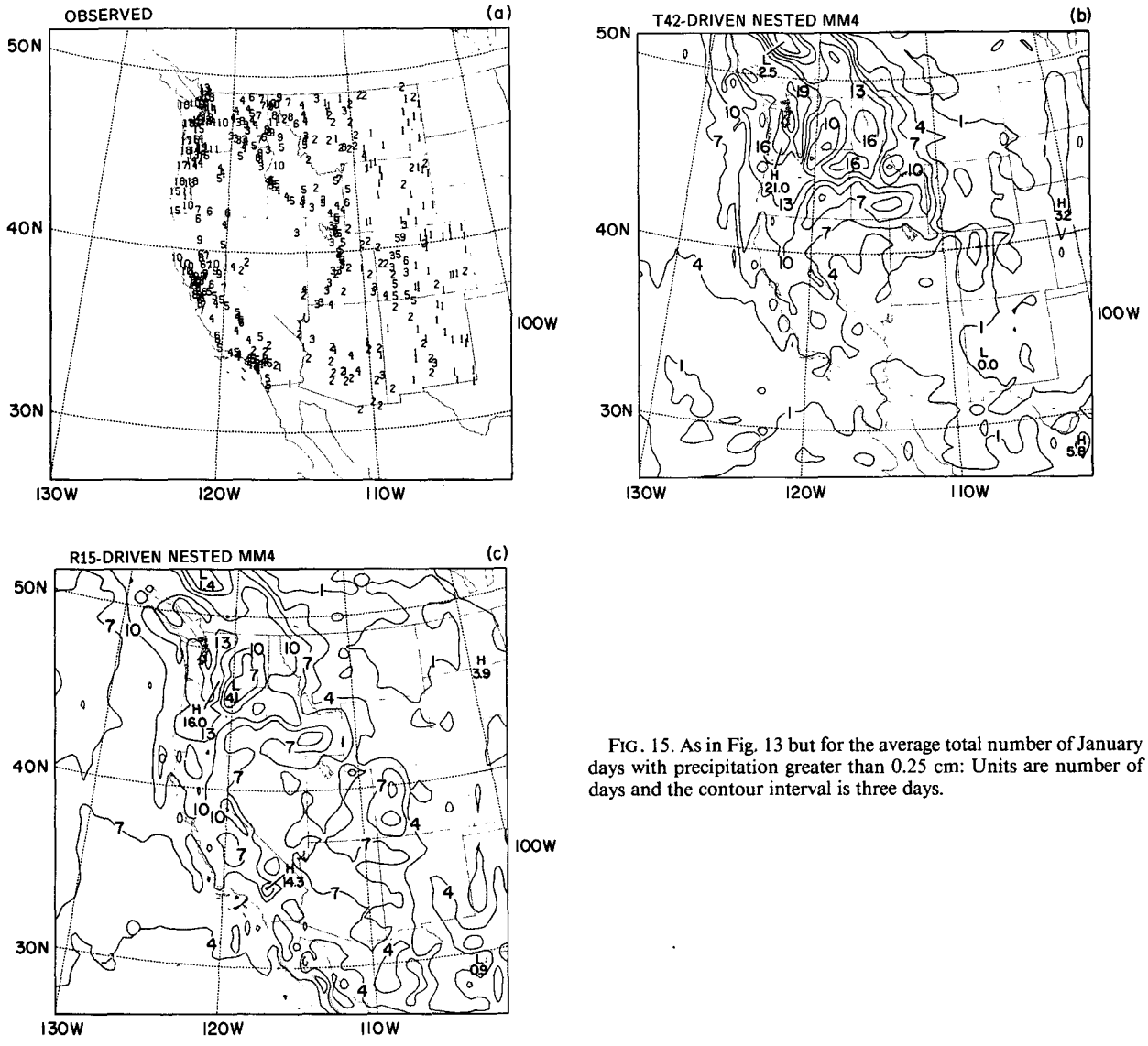

FIG. 15. As in Fig. 13 but for the average total number of January days with precipitation greater than 0.25 cm: Units are number of days and the contour interval is three days.

rounding to the closest integer. Also note that the comparison is not strictly rigorous, since the model data refer to 60 × 60 km^2 spatial averages, while the observed data refer to individual stations.

For the lowest precipitation threshold of 0.25 cm, observations show intensity frequencies of 1–3 day/month over most of Montana, Wyoming, eastern Colorado, Utah, New Mexico, Nevada and Arizona. The frequencies increase to 4–7 day/month over the Rockies of Colorado and central Arizona, the Wasatch Range, southern Idaho, eastern Oregon and Washington, and areas of northern and southern California. Frequencies of 7–10 day/month are observed over the Sierra Nevada and the coast of central California, northern Idaho Rockies and Colorado Rockies. Finally, over the coasts of the Pacific Northwest, the frequencies exceed 10 day/month and reach 18 day/month. The T42-driven simulation reproduces most of these observed features but overestimates the frequencies in the northwestern States. The R15-driven simulation overestimates frequencies also over the Southwest.

As the daily precipitation threshold increases, the agreement between models and observations improves. For a threshold of 1.25 cm both the T42-driven model results and the station database show areas with frequencies of 1–3 day/month in the Rockies and southern California, 3–5 day/month over central and northern coastal regions, and higher than 5 day/month over northern California, Oregon, and Washington. Again, the R15-driven model results show spatial patterns in agreement with observations but overestimate frequencies in the southwestern States. Finally, both models correctly predict frequencies of daily precipitation over 2.5 cm in the range 1–3 day/month along

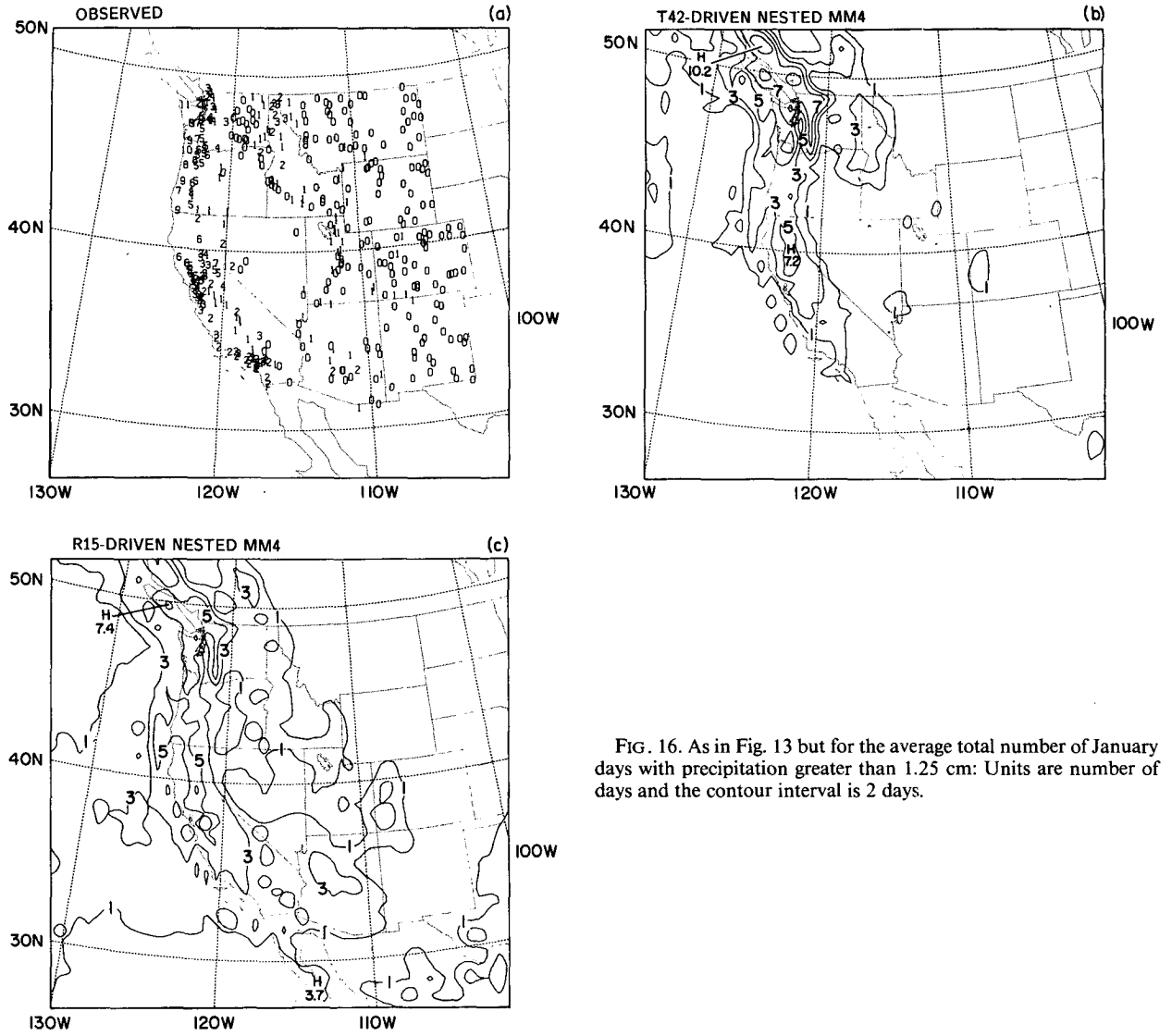

FIG. 16. As in Fig. 13 but for the average total number of January days with precipitation greater than 1.25 cm: Units are number of days and the contour interval is 2 days.

the western coasts, and frequencies of more than 3 day/month over isolated areas of northern California and the Pacific Northwest.

Figures 14–17 thus indicate that the nested model system is capable of reproducing realistic high resolution patterns not only of average precipitation but also of frequencies of precipitation intensities. In this regard, an interesting feature can be inferred from the storm frequency analysis of section 3 and the precipitation intensity frequencies of Figs. 15–17. Namely, while the R15 model underpredicts storm events, it overpredicts the number of rainy days. This implies that, compared to observations and to the T42 model, precipitation in the R15 model is produced by a relatively small number of slow and strong disturbances.

The January total average cloud cover predicted by the T42-driven and R15-driven MM4 simulations is shown in Figs. 18a, b. In the MM4 the fractional cloud cover at a given grid point (f_{cl}) is diagnostically calculated as a function of relative humidity (RH) using the formula

$$f_{cl} = \left(\frac{\mathrm{RH} - 0.8}{0.2}\right)^2$$

for RH greater than 0.8 and $f_{cl} = 0$ for RH lower than 0.8 (Slingo 1980), which allows for the occurrence of fair weather cloudiness. As for the CCM1, the total column cover is calculated with the assumption of random overlap.

The nested MM4 average cloud covers show large-scale features similar to those of the driving CCM runs; i.e., larger cloud covers for the T42-driven than the R15-driven run over the Pacific Northwest, and smaller over the Southwest. Significant regional detail, however, is produced by the orographic uplift associated

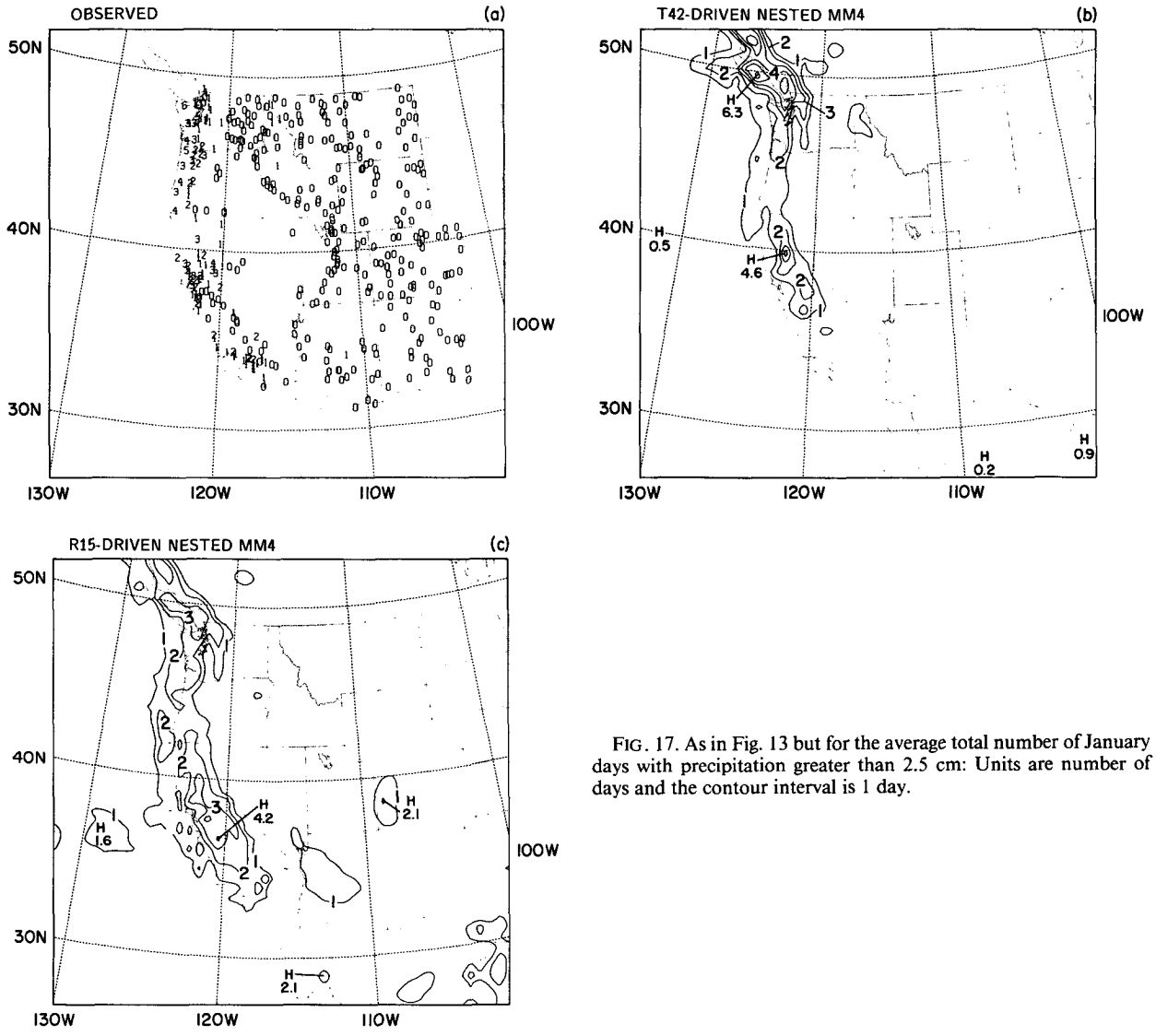

FIG. 17. As in Fig. 13 but for the average total number of January days with precipitation greater than 2.5 cm: Units are number of days and the contour interval is 1 day.

with the MM4 topography. In the T42-driven run, maximum fractional covers exceeding 80% are found over the Cascade Range and the Idaho Rockies, while over the central Rockies and Sierra Nevada mountains cloudiness is enhanced significantly compared to the surrounding regions. In the southwestern States cloudiness is very low, with average fractional covers in the range of 10%–30%. In the R15 simulation the average fractional cover is above 30% over the whole domain, with maxima of 70% over the northern Rockies and the Cascade range and exceeding 50% over central and southern Rockies and the Sierra Nevada.

Although orographic enhancement of cloudiness can be expected, high resolution observations of cloud climatology necessary to verify the extent of this effect are not yet available. Such data may become available in the future from high resolution remote sensing measurements.

One of the most interesting characteristics of the application of BATS to climate and hydrology studies is its capability of predicting snowpack formation. The snow depth is prognostically calculated in BATS from the mass balance of snowfall, sublimation, and melting, and in the MM4 simulations it is initialized by interpolation from the CCM1 snow depth. In the standard CCM1 used here, the snow depth is not calculated but is specified as a function of season and latitude. For January conditions, the snow depth is specified to be equal to 1 cm of liquid water over land areas north of about 42°N, the initial value likewise assumed for the MM4.

Climatological snow depth observations are currently not available, but average snow cover frequencies derived from 15 years (1967–81) of satellite observations are reported in the NOAA Atlas (1986) on a grid with resolution varying in the range 16 000–42 000

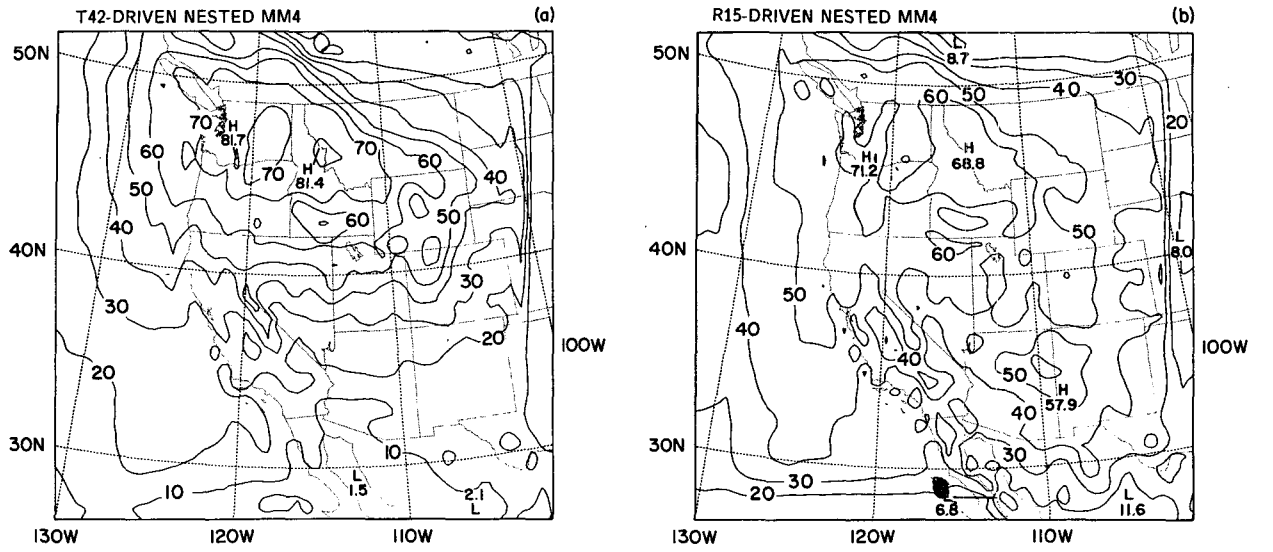

FIG. 18. As in Fig. 13 but for the average January fractional cloud cover for nested MM4 simulations: Units are % and the contour interval is 10%.

km^2. The frequencies are given in percentage of number of weeks within a given month in which fractional snow cover area was observed to be in excess of 50%. To compare with observations, model snow covers were obtained from the snow depths using the formula adopted in BATS for snow albedo calculations, in which the fractional snow cover area is proportional to the ratio of snow depth and height of the surface elements (Dickinson et al. 1986). MM4 snow cover frequencies averaged over the six T42-driven and R15-driven Januaries were then calculated on the MM4 grid by assuming, as in the NOAA Atlas (1986), that a grid box is covered by snow if the fractional snow cover area is greater than 50%. Only model data on 0000 UTC 31 January, i.e., at the end of the MM4 runs, were considered in order to minimize the impact of the assumption of initial MM4 snow depths of 1 cm for areas north of 42°, which was obtained from the interpolation of the CCM1 snow depth field. This assumption is clearly unrealistic on the regional scale.

Figures 19a–c compare observed and modelproduced snow cover frequencies. Overall, the agreement between models and observations is quite good. In both cases the 10% frequency limit crosses northwestern New Mexico, central Arizona, southern Nevada, western California, Oregon and Washington. Over most of Idaho, Montana, Wyoming, and the central Rockies both models and observations show frequencies in excess of 80%. Over the Sierra Nevada and the Cascade Range, the models predict 50–100% frequencies versus the 70–80% shown by the observed dataset, while over the central and northern Great Basin, model as well as observed values show a northward increase from about 20% to about 80%.

In summary, due to the better representation of the western United States topography, the nested MM4 produces much more realistic regional detail of temperature, precipitation, and snow cover distribution than the driving CCM1 alone and shows good agreement with available high resolution observations. In the next section, we will discuss in more detail the regional hydrologic budgets simulated by the nested MM4 for the western United States.

5. Simulated hydrologic budgets for different regions of the western United States

The augmented MM4 includes a detailed soil hydrology package which explicitly predicts, in addition to snow depth, the soil water content of a top soil layer (of 10 cm thickness) and that of a root zone layer (of 1–2 m thickness), surface runoff, root zone drainage and evapotranspiration (Dickinson et al. 1986). The soil water movement formulations are based on high resolution soil model calculations (Dickinson 1986), with the soil water diffusivity being a nonlinearly increasing function of soil water content relative to saturation. Surface runoff rates are proportional to the soil water content relative to saturation and to the precipitation rates. Evapotranspiration calculations include the representation of a canopy layer with parameterized stomatal pore physics. In this section we discuss the soil hydrologic budget simulated by the nested MM4 for different regions of the western United States as they relate to local precipitation regimes.

Tables 1 and 2 show the 30-day accumulated January values of the various components of the surface hydrologic budget for the T42- and R15-driven simulations and for six regions of the western United States: the Pacific Northwest (Washington and Oregon), California, the Great Basin (Nevada and western Utah), the Northern Rockies (Idaho, Montana, and Wyo-

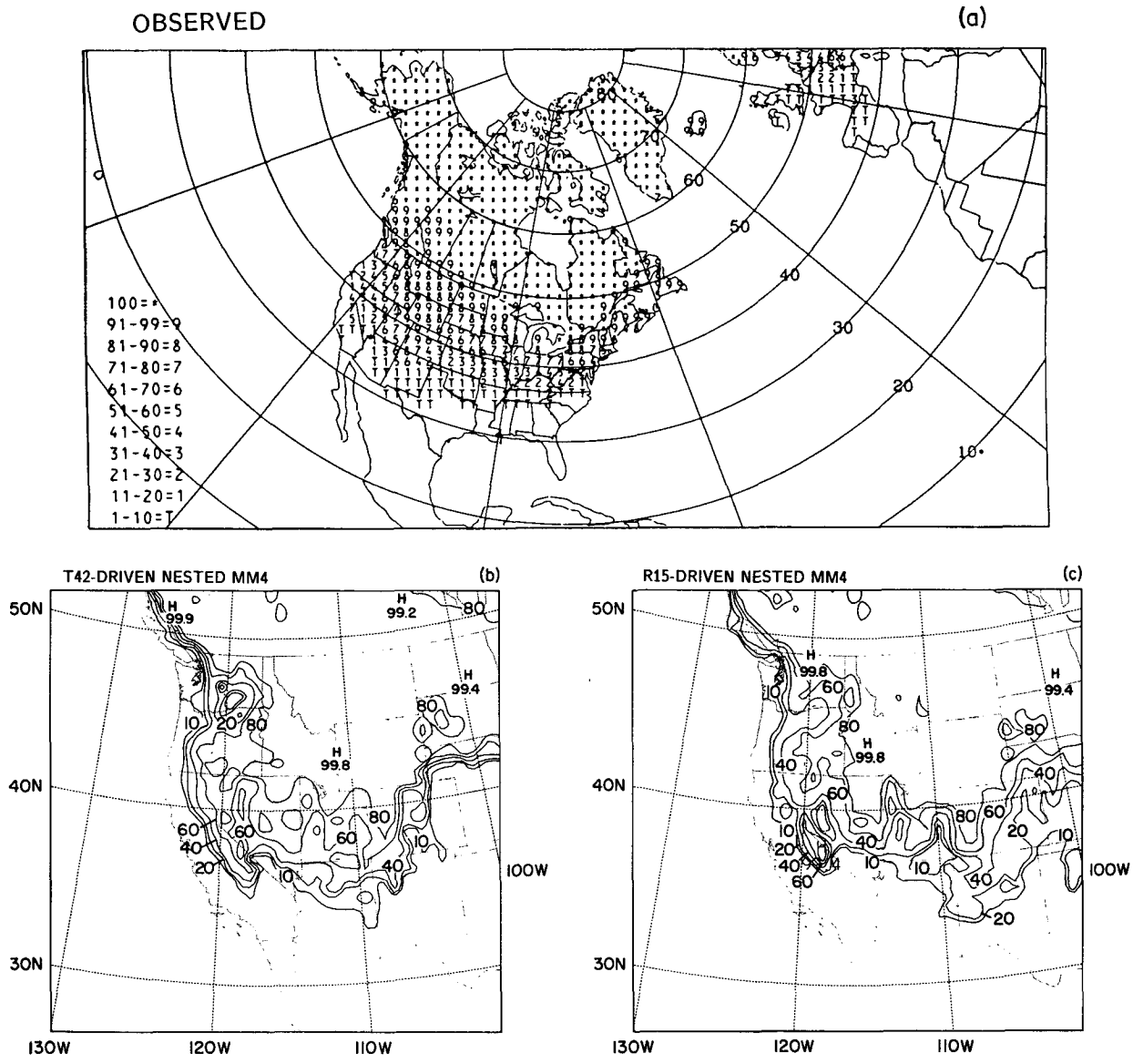

FIG. 19. Average January snow cover frequency (see text): (a) Observations (from the NOAA Atlas 1986); (b) T42-driven nested MM4; (c) R15-driven nested MM4. Units are %. Observed frequency ranges are defined in the legend, in (b) and (c) the contour interval is 20%.

ming), the Central Rockies (Colorado and eastern Utah), and the Southern Rockies (New Mexico and Arizona). Also presented are the soil water contents relative to saturation at the end of the January runs. These are reported in place of the water contents because both the calculated surface runoff and root zone drainage depend on the water content relative to saturation. The domain is subdivided into six regions because the climate and hydrology of each region are subject to different orographic forcings, precipitation climatology, and soil conditions. Averages over six simulated months, as well as the lowest and highest monthly values, are presented. The latter give an estimate of the simulated interannual variability and are used in place of a more standard measure of variability (such as, for example, the standard deviation) because of the small sample considered. The values for a given region are obtained by averaging over all the MM4 grid points within that region.

Analyzing first the T42-driven simulation, the Pacific Northwest and California receive the largest amounts of precipitation with averages of 13.55 cm/month and 7.33 cm/month, respectively, while the southern Rockies, central Rockies, and Great Basin receive an average of less than 3.5 cm/month. These results are consistent with the orographically modulated precip-

TABLE 1. Final water content relative to saturation for the root zone (w_s), and average January accumulated precipitation, evaporation, surface runoff, snow depth (in equivalent cm of liquid water), and root zone drainage over six regions of the western United States, for T42-driven nested MM4 simulation. The top value of each set of three gives the maximum monthly value, the middle value gives the average over six simulated Januaries, and the bottom value gives the minimum monthly value.

Pacific Northwest	California	Great Basin	Northern Rockies	Central Rockies	Southern Rockies
		w_s			
0.93	0.60	0.49	0.96	0.56	0.48
0.87	0.54	0.47	0.96	0.56	0.48
0.80	0.48	0.45	0.96	0.56	0.47
		Precipitation (cm)			
15.86	17.87	8.91	6.75	6.14	2.41
13.55	7.33	3.32	4.62	2.65	1.12
9.04	0.23	0.74	2.88	1.42	0.20
		Evaporation (cm)			
1.54	2.14	1.89	1.00	1.02	1.33
1.38	1.97	0.83	0.66	0.89	1.19
0.90	1.73	0.74	0.40	0.77	1.02
		Surface Runoff (cm)			
8.81	5.68	1.47	0.98	0.30	0.80
7.13	2.05	0.62	0.75	0.18	0.29
3.12	0.07	0.22	0.12	0.06	0.05
		Snow Depth (cm)			
6.15	3.75	5.03	6.16	5.03	0.72
3.41	1.21	1.56	4.35	1.97	0.19
1.54	0.01	0.07	2.46	0.69	0.01
		Drainage (cm)			
22.12	8.93	1.54	1.05	0.30	0.88
17.18	3.80	0.63	0.87	0.18	0.36
8.52	1.07	0.23	0.12	0.06	0.10

itation field of Fig. 14. In addition, the southwestern regions (California, Great Basin, and southern Rockies) show a much higher range of monthly precipitation than the northwestern ones. In the former, January precipitation varies within a range of two orders of magnitude between maximum and minimum values, while in the latter it varies only by a factor of 1.5–4. This is due to the fact that, in two of the six simulated months, the jet remained over the Northwest throughout the whole period and never moved over the southwestern States.

Over the northern Rockies most of the precipitation accumulates in the form of snow. Note that the initial snow depth of one equivalent centimeter of liquid water for areas above a latitude of 42°N should be taken into consideration in the snow depth averages of Tables 1 and 2. Snow accumulation represents a significant fraction of the total precipitation also over the Pacific Northwest, California, the central Rockies, and the Great Basin, while over the southern Rockies most precipitation is in the form of rain, and any falling snow rapidly melts. The interannual ranges of monthly snow depths are larger than the ranges of precipitation, suggesting that during months of high snowfall, surface temperatures are relatively low and snowmelt less efficient.

Because the surface runoff rates calculated in BATS are directly proportional to the soil water content relative to saturation and the rainfall rates, runoff is maximum over the wettest regions; i.e., the Pacific Northwest and California, where it accounts for 30%–50% of the total precipitation. Over the other regions it is a minor component of the soil hydrologic budget. The interannual ranges of monthly values follow the same

TABLE 2. Final water content relative to saturation for the root zone (w_s), and average January accumulated precipitation, evaporation, surface runoff, snow depth (in equivalent cm of liquid water), and root zone drainage over six regions of the western United States, for R15-driven nested MM4 simulation. The top value of each set of three gives the maximum monthly value, the middle value gives the average over six simulated Januaries, and the bottom value gives the minimum monthly value.

Pacific Northwest	California	Great Basin	Northern Rockies	Central Rockies	Southern Rockies
		w_s			
0.93	0.68	0.70	0.96	0.72	0.57
0.88	0.62	0.65	0.96	0.71	0.52
0.80	0.54	0.61	0.96	0.70	0.47
		Precipitation (cm)			
15.73	24.19	12.66	4.44	9.76	11.98
12.47	15.08	6.92	3.98	5.40	5.74
6.08	4.06	1.75	2.18	1.29	2.63
		Evaporation (cm)			
1.79	2.54	1.47	0.66	1.26	2.41
1.37	2.37	1.14	0.58	1.05	1.87
0.78	1.65	0.77	0.28	0.79	0.95
		Surface Runoff (cm)			
9.87	10.00	4.75	1.02	2.12	4.05
6.80	5.76	3.07	0.82	1.29	1.69
2.64	0.93	0.73	0.26	0.27	0.14
		Snow Depth (cm)			
4.86	1.62	2.60	4.09	6.44	0.55
2.94	0.78	1.11	3.79	3.21	0.19
1.21	0.12	0.17	2.16	0.74	0.01
		Drainage (cm)			
25.70	17.51	6.62	2.37	2.19	5.57
15.68	10.87	4.09	0.93	1.27	2.45
4.30	3.64	1.13	0.26	0.27	0.15

patterns as those discussed for the precipitation amounts.

As expected, evaporation is strongest in the warmest and wettest regions of the domain: the Pacific Northwest, California, and the southern Rockies. Because of the low surface temperatures, the evaporative fluxes are minimum over the northern Rockies. Over the southern Rockies the soil water loss due to evaporation exceeds the precipitation input (i.e., precipitation minus snow depth and surface runoff in Tables 1 and 2), while in the other regions, except the northern Rockies, it is 30%–40% of the precipitation input. Evidently, even in wintertime, when the evaporative fluxes are minimum, evapotranspiration is an important component of the soil moisture budget over most of the western United States. Because the evaporation rates depend mainly on temperature and soil moisture, which are generally less variable than precipitation, evapotranspiration contains a lower degree of interannual variability. Monthly values generally vary within a factor of 0.25% of the multiyear average.

Because the soil water diffusivity is a nonlinearly increasing function of the soil water content relative to saturation (e.g., Dickinson et al. 1986), root zone drainage is strongly dependent on the degree of soil wetness. The correlation between soil wetness and root zone drainage is quite evident except over the northern and southern Rockies, where the soil is frozen over most areas. Ground freezing prevents soil water movement and reduces root zone drainage. Over the Pacific Northwest, where the initial soil water content is close to saturation and the soil is not frozen, gravitational drainage strongly dominates the water budget of the root zone. Over California, drainage is a main component of the budget, while over the Great Basin and the southern Rockies, the driest regions in the domain, it is small.

Root zone drainage shows a high degree of interannual variability for all regions, with a factor of 3–9 difference between highest and lowest monthly totals. This can be attributed to the highly nonlinear response of soil water diffusivity to soil water content. Changes in monthly precipitation produce relatively small changes in soil water content relative to saturation, which in turn are amplified by the nearly exponential dependence of soil water diffusion on soil wetness. Note that this process also contributes to prevent large month-to-month variations in soil moisture content.

Finally, the water balance of the root zone is regulated by the input from rainfall and snowmelt (minus the fraction that is lost through runoff) and the loss due to evapotranspiration and gravitational drainage. In the Pacific Northwest the drainage loss dominates the water budget, and a net average drying of about 14.5 cm takes place. Similarly, the California soil undergoes a net drying of 1.7 cm, to which evapotranspiration is also an important contributor. In the Great Basin the water budget tends to balance on average, although, as for California, the budget for individual months varies considerably due to the high variability of the precipitation input. Over the northern and central Rockies the extended ground freezing inhibits soil water cycling, while over the southern Rockies the low precipitation amounts predicted by the T42-driven simulation yield an average drying of about 3 cm.

Considering now the R15-driven model, the main difference between the R15-driven and the T42-driven simulations consists of a southward shift of the R15-simulated jet with respect to the jet in the T42 simulation. This induces larger precipitation and runoff amounts in the R15-driven runs over the central and southern Rockies, Great Basin and California.

Another significant difference between the R15-driven and the T42-driven models is associated with the initial snow depth distribution. Because of the different resolutions of the R15 and T42 models, the interpolation to the MM4 grid leads to initial snow depths of 1 cm of liquid water over land areas north of 40°N for the R15-driven model and north of 42°N for the T42-driven model. As a result, areas of northern California, the Great Basin, and central Rockies that are initially snow-free in the T42-driven simulations are covered with snow in the R15-driven runs. Because the initial soil water content is set equal to saturation over snow-covered land areas, the initial soil moisture for these southwestern regions is larger in the R15-driven model than in the T42-driven model. This in turn leads to larger soil water contents relative to saturation and root zone drainage totals for the R15-driven model as shown in Tables 1 and 2. Also note the generally lower snow depths over the Southwest predicted by the R15-driven runs compared to the T42-driven ones. These are due to higher surface temperatures (see Fig. 13) and enhanced snowmelt. The higher temperatures and soil moisture contents in the R15-driven simulations also lead to higher evapotranspiration totals.

The water budget of the root zone for the Pacific Northwest and the northern Rockies is similar in the R15-driven and T42-driven models. Over the southwestern regions the R15-driven model predicts higher precipitation inputs, but also more efficient runoff and soil water loss mechanisms. Consequently, the Southwest on average still undergoes drying, but this is less pronounced than in the T42-driven simulation.

6. Summary and conclusions

This paper presents an example of applying a nested LAM–GCM model system to regional climate simulation. In the nested modeling approach, the coarse resolution GCM is first used to simulate the large-scale response of the global circulation to global climatic forcings or impacts. The output from the GCM simulation is then used to drive a high resolution LAM over an area of interest in order to capture sub-GCM grid scale forcings, such as those due to complex to-

pography and large bodies of water, that may substantially affect the local climate. The development of this methodology is still at its early stages and this paper addresses some of the issues and possible problems concerning its use. This is accomplished by discussing results from the application of the NCAR CCM1 Global Climate Model and an augmented version of the Penn State/NCAR mesoscale model (which includes soil hydrology calculations) to the simulation of January climatology over the western United States.

The western United States is one of the regions for which the nested modeling approach can be most useful because the complexity of local topographical features, which strongly affects the regional distribution of climatic variables such as temperature and precipitation, is not captured at the resolution of most GCMs. The output from multiyear seasonal CCM1 simulations at R15 (4.5° × 7.5° latitude–longitude) and T42 (2.89° × 2.89° latitude–longitude) resolution was used to drive the MM4 at 60 km grid point spacing over a domain covering the western United States and adjacent ocean waters.

The CCM1-simulated large-scale January climate over the western United States was analyzed first. Both the R15 and T42 models effectively simulated the large-scale average circulations over the region as well as large-scale patterns of precipitation and surface air temperature. The T42 model, however, captured better than the R15 model storm frequencies and the intensity and location of the jet stream.

A number of month-long January simulations were performed with the nested MM4 driven by both the R15 and the T42 outputs. The large-scale January climate simulated by the nested MM4 over the model domain was not substantially different from that of the driving CCM1. This suggests the need of using a good large-scale driving climatology for successful simulation of regional climates via LAM nesting, although more tests are needed to confirm this conclusion. Our results also showed that the nesting procedure is not sensitive to the resolution of the driving GCMs in terms of mean error generation.

Owing to its better representation of the western United States topography, the nested MM4 produced much more realistic regional detail of the temperature and precipitation distribution than the CCM alone. Temperature and precipitation means, as well as frequencies of daily precipitation intensities as simulated by the nested model, compare well with high resolution station observations, especially in their spatial distribution.

Also discussed in the paper are the snow cover and cloud distribution and the soil hydrologic budgets simulated by the augmented MM4 for different regions of the western United States. These appear realistic in many respects, although verification at the present model resolution is difficult.

The results presented here indicate that, with the use of a good large-scale driving climatology, the nested model system can simulate accurate regional climatic detail. Although global models of increasingly higher resolution continue to be developed, it is likely that coarse resolution GCMs will remain the primary tools for climatic change projections for the next several years. This is the case, for example, of projections of climatic change due to increases in greenhouse gas concentrations, for which coupled ocean, sea ice, and atmospheric models need to be developed and long simulations need to be performed. The nested modeling technique can thus provide a useful tool for achieving accurate regional climate detail for areas where high resolution local climate forcings are important. Although computationally demanding, this technique employs currently available and well tested tools, i.e., coarse resolution GCMs and high resolution LAMs, and can be carried out with currently available computational resources. Even when high resolution GCMs become available, this technique may be useful for specific studies.

The next step in the nested model development will consist of analysis and testing similar to that presented here but for different seasons, with the long term purpose of applying the model to the generation of regional climatic change scenarios. Areas other than the western United States are currently under investigation for application of the nested CCM/MM4 model system. These include the Great Lakes Basin, southeastern Australia, and Western Europe.

Acknowledgments. I would like to thank R. Dickinson, G. Bates, and R. Errico for useful discussions and suggestions throughout the completion of this work, and the anonymous reviewers for their thorough reviews of the manuscript.

REFERENCES

Anthes, R. A., 1983: Regional models of the atmosphere in middle latitudes. *Mon. Wea. Rev.*, **111,** 1306–1335.

——, 1977: A cumulus parameterization scheme utilizing a one-dimensional cloud model. *Mon. Wea. Rev.*, **105,** 270–286.

——, and T. T. Warner, 1978: Development of hydrodynamical models suitable for air pollution and other mesometeorological studies. *Mon. Wea. Rev.*, **106,** 1045–1078.

——, E. Y. Hsie and Y. H. Kuo, 1987: Description of the Penn State/NCAR Mesoscale Model Version 4 (MM4). NCAR Tech. Note, NCAR/TN-282+STR, 66 pp.

Blackmon, M. L., J. M. Wallace, N. C. Lau and S. Mullen, 1977: An observational study of the Northern Hemisphere wintertime circulation. *J. Atmos. Sci.*, **34,** 1040–1053.

Climates of the States, 1985a: *Volume I, Alabama-New Mexico.* NOAA, Gale Research Company, 758 pp.

——, 1985b: *Volume II, New York-Wyoming, Appendices.* NOAA, Gale Research Company, 814 pp.

Dickinson, R. E., 1986: The climate system and modeling of future climate. *The Greenhouse Effect, Climatic Change, and Ecosystems.* B. Bolin, B. R. Doos, J. Jager and R. A. Warrick, Eds., SCOPE, 207–270.

——, P. J. Kennedy, A. Henderson-Sellers and M. Wilson, 1986: Biosphere–Atmosphere Transfer Scheme (BATS) for the NCAR Community Climate Model. NCAR Tech. Note, NCAR/TN-275+STR, 69 pp.

——, R. M. Errico, F. Giorgi and G. T. Bates, 1989: A regional climate model for the western U.S. *Climatic Change,* **15,** 383–422.

Giorgi, F., 1990: Sensitivity of wintertime precipitation and soil hydrology simulation over the western United States to lower boundary specification. *Atmos. Ocean,* **28,** 1–23.

——, and G. T. Bates, 1989: On the climatological skill of a regional model over complex terrain. *Mon. Wea. Rev.,* **117,** 2325–2347.

——, ——, R. M. Errico and R. E. Dickinson, 1989: Modeling the climate of the western United States with a limited area model coupled to a general circulation model. Proc., *Sixth Conf. on Applied Climatology,* Charleston, 201–208.

Hosler, D. L., and L. A. Gamage, 1956: Cyclone frequencies in the United States for the period 1905–1954. *Mon. Wea. Rev.,* **84,** 388–390.

Kiehl, J. T., R. J. Wolski, B. P. Briegleb and V. Ramanathan, 1987: Documentation of radiation and cloud routines in the NCAR Community Climate Model (CCM1). NCAR Tech. Note, NCAR/TN-288+IA, 109 pp.

Klein, W. H., 1957: Principal tracks and mean frequencies of cyclones and anticyclones in the Northern Hemisphere. Res. Pap. No. 40, U.S. Weather Bureau, 60 pp.

Legates, D. R., and C. J. Willmott, 1990a: Mean seasonal and spatial variability in global surface air temperature. *Theor. Appl. Climate,* in press.

——, and ——, 1990b: Mean seasonal and spatial variability in gage-corrected global precipitation. *Int. J. Climatol.,* in press.

Malone, R. C., E. J. Pitcher, M. L. Blackmon, K. Puri and W. Bourke, 1984: The simulation of stationary and transient geopotential-height eddies in January and July with a spectral general circulation model. *J. Atmos. Sci.,* **41,** 1394–1419.

Mearns, L. O., R. W. Katz and S. H. Schneider, 1984: Extreme high-temperature events: Changes in their probabilities with changes in mean temperature. *J. Climate Appl. Meteor.,* **23,** 1601–1613.

——, S. H. Schneider, S. L. Thompson and L. R. McDaniel, 1990: Analysis of climate variability in general circulation models: Comparison with observations and changes in variability in 2 $\times$ CO_2 experiments. *J. Geophys. Res.,* in press.

NOAA Atlas, 1986: *An Atlas of Satellite-Derived Northern Hemispheric Snow Cover Frequency.* U.S. Dept. of Commerce, 75 pp.

Pitcher, E. J., R. C. Malone, V. Ramanathan, M. L. Blackmon, K. Puri and W. Bourke, 1983: January and July simulations with a spectral general circulation model. *J. Atmos. Sci.,* **40,** 580–604.

Ramanathan, V., E. J. Pitcher, R. C. Malone and M. L. Blackmon, 1983: The response of a spectral general circulation model to refinements in radiative processes. *J. Atmos. Sci.,* **40,** 605–630.

Reitan, C. H., 1974: Frequencies of cyclones and cyclogenesis for North America, 1952–1970. *Mon. Wea. Rev.,* **102,** 861–868.

——, 1979: Trends in the frequencies of cyclone activity over North America. *Mon. Wea. Rev.,* **107,** 1684–1688.

Shea, D. J., 1986: Climatological Atlas: 1950–1979. Surface air temperature, precipitation, sea-level pressure, and sea-surface temperature (45°S–90°N). NCAR Tech. Note, NCAR/TN-269+STR, 35 pp.

Slingo, J. M., 1980: A cloud parameterization scheme derived from GATE data for use with a numerical model. *Quart. J. Roy. Meteor. Soc.,* **106,** 341–362.

Taylor, K. E., 1986: An analysis of the biases in traditional cyclone frequency maps. *Mon. Wea. Rev.,* **114,** 1481–1490.

Trenberth, K. E., and J. G. Olson, 1988: ECMWF Global analyses 1979–1986: Circulation statistics and data evaluation. NCAR Tech. Note, NCAR/TN-300+STR, 94 pp.

Warren, S. G., C. J. Hahn, J. London, R. M. Chervin and R. L. Jenne, 1986: Global distribution of total cloud cover and cloud type amounts over land. NCAR Tech. Note, NCAR/TN-273+STR, 29 pp.

Williamson, G. S., and D. L. Williamson, 1987: Circulation statistics from seasonal and perpetual January and July simulations with the NCAR Community Climate Model (CCM1):R15. NCAR Tech. Note, NCAR/TN-302+STR, 200 pp.

Williamson, D. L., J. T. Kiehl, V. Ramanathan, R. E. Dickinson and J. J. Hack, 1987: Description of NCAR Community Climate Model (CCM1). NCAR Tech. Note, NCAR/TN-285+STR, 112 pp.

Zishka, K. M., and P. J. Smith, 1980: The climatology of cyclones and anticyclones over North America and surrounding ocean environs for January and July, 1950–77. *Mon. Wea. Rev.,* **108,** 387–401.